



Article

# Hijacking Sexual Immuno-Privilege in GBM—An Immuno-Evasion Strategy

Martyn A. Sharpe <sup>1,\*</sup> , David S. Baskin <sup>1,2</sup>, Amanda V. Jenson <sup>1</sup> and Alexandra M. Baskin <sup>1</sup>

<sup>1</sup> Kenneth R. Peak Brain and Pituitary Tumor Treatment Center, Department of Neurosurgery, Houston Methodist Neurological Institute, Houston Methodist Hospital and Research Institute, Houston, TX 77030, USA; dbaskin@houstonmethodist.org (D.S.B.); avjenson@houstonmethodist.org (A.V.J.); ambaskin@houstonmethodist.org (A.M.B.)

<sup>2</sup> Department of Neurological Surgery, Weill Cornell Medical College, New York, NY 10065, USA

\* Correspondence: masharpe@houstonmethodist.org

**Abstract:** Regulatory T-cells (Tregs) are immunosuppressive T-cells, which arrest immune responses to ‘Self’ tissues. Some immunosuppressive Tregs that recognize seminal epitopes suppress immune responses to the proteins in semen, in both men and women. We postulated that GBMs express reproductive-associated proteins to manipulate reproductive Tregs and to gain immune privilege. We analyzed four GBM transcriptome databases representing  $\approx 900$  tumors for hypoxia-responsive Tregs, steroidogenic pathways, and sperm/testicular and placenta-specific genes, stratifying tumors by expression. In silico analysis suggested that the presence of reproductive-associated Tregs in GBM tumors was associated with worse patient outcomes. These tumors have an androgenic signature, express male-specific antigens, and attract reproductive-associated Related Orphan Receptor C (RORC)-Treg immunosuppressive cells. GBM patient sera were interrogated for the presence of anti-sperm/testicular antibodies, along with age-matched controls, utilizing monkey testicle sections. GBM patient serum contained anti-sperm/testicular antibodies at levels > six-fold that of controls. Myeloid-derived suppressor cells (MDSCs) and tumor-associated macrophages (TAMs) are associated with estrogenic tumors which appear to mimic placental tissue. We demonstrate that RORC-Tregs drive poor patient outcome, and Treg infiltration correlates strongly with androgen levels. Androgens support GBM expression of sperm/testicular proteins allowing Tregs from the patient’s reproductive system to infiltrate the tumor. In contrast, estrogen appears responsible for MDSC/TAM immunosuppression.

**Keywords:** GBM; HiF; Tregs; microglia; androgen; estrogen; sperm; testicular; myeloid-derived suppressor cells; tumor-associated macrophages



**Citation:** Sharpe, M.A.; Baskin, D.S.; Jenson, A.V.; Baskin, A.M. Hijacking Sexual Immuno-Privilege in GBM—An Immuno-Evasion Strategy. *Int. J. Mol. Sci.* **2021**, *22*, 10983. <https://doi.org/10.3390/ijms222010983>

Academic Editor: Salvatore Coniglio

Received: 20 August 2021

Accepted: 5 October 2021

Published: 12 October 2021

**Publisher’s Note:** MDPI stays neutral with regard to jurisdictional claims in published maps and institutional affiliations.



**Copyright:** © 2021 by the authors. Licensee MDPI, Basel, Switzerland. This article is an open access article distributed under the terms and conditions of the Creative Commons Attribution (CC BY) license (<https://creativecommons.org/licenses/by/4.0/>).

## 1. Introduction

Despite aggressive treatment, the median survival of GBM patients is only  $\approx 15$  months [1–3] and less than 5% survive  $\geq 5$  years postdiagnosis [1,4]. Swanson and colleagues’ computational tools estimate patient survival based on temporally distant T1-contrasted and T2-FLAIR images. They found long-term survivors of GBM (>36 months) tend to have slow-growing diffuse tumors with high T1-contrast and high FLAIR signal, whereas short-term survivors (<19 months) tend to have fast-growing focal tumors with little FLAIR signal [5,6]. Huang and colleagues recently demonstrated small hypoxic tumors display little FLAIR signal and correlate with poor outcome, confirming Swanson’s work [5–7]. The switch from aerobic to anaerobic respiration in cancers results from elevation of active hypoxia-inducible factor 1 $\alpha$  (HiF) levels [8]. This activates transcription of hypoxia response genes, including Glut1 (*SLC2A1*) [9], Glut3 (*SLC2A3*) [10,11], *VEGFA* [12], *VLDLR* [13], and *ADM* [14]. Hypoxia, and the activation of HiF responsive genes in immune cells is well known to alter their function [15].

The response of the patient immune system to the GBM also affects patient outcome, with poor outcome being associated with tumor infiltration of myeloid-derived suppressor cells (MDSC) [16,17], tumor-associated macrophages (TAM) [18,19] and regulatory T-cells (Tregs) [20,21]. There may be a link between GBM tumor hypoxia and MDSCs and immunosuppressive macrophages. These are typically localized uterocervically, an area characterized by low glucose, low oxygen, low pH, and high lactate levels, much like a hypoxic tumor. Many of the components that induce uterocervical colonization by MDSCs/macrophages and their immunosuppressive phenotypes are also typically found in tumors, including GBM [22].

The levels of mRNA or protein markers of Treg infiltration into GBM tumors have been linked with poor outcome, including Forkhead Box P3 (*FOXP3*) [23], Cytotoxic T-Lymphocyte-Associated Protein 4 (*CTLA4*) [24,25], glucocorticoid-induced TNFR-related protein (*GITR*, (the *TNFRSF18* gene product)) [20,26] and GATA-binding protein 3 (*GATA3*) [27].

Th17-derived Tregs express the Related Orphan Receptor C (RORC) [28], along with *FOXP3*, *CTLA4*, and *GITR* [29]. These RORC-Tregs generally colonize mucin-rich tissues including in the gastrointestinal tract (GI) and kidney [29–32]. Additionally, the adult male and female reproductive tracts are lined with membrane-bound mucins and coated with soluble mucins, with levels of MUC1, 4 and 5AC elevated by androgen and estrogen. In these reproductive tissues the mucosal layer is infiltrated with Tregs [33,34].

MUC16 is a membrane-bound protein which generates a soluble mucin following proteolytic action, with the solubilized fragment sometimes called carcinoma antigen-125 (CA-125). Uterocervical CA-125 is generated in situ from MUC16 expressed in the cervix/uterus/endometrium [35] and high levels are an indicator of endometrial receptivity and a predictor of pregnancy [36]. Uterocervical CA-125 levels can be directly augmented from a sexual partner as seminal plasma has high levels of CA-125 [37]. This mucin fragment drives epitope-specific Treg infiltration and activation in normal reproductive biology and cancer, with CA-125 also expressed by ovarian tumors, generating an immunosuppressive niche [38]. The physiological function of the uterocervical RORC-Treg population is to aid the granting of immuno-privilege to ‘non-Self’ male-specific, partner-specific and offspring-specific seminal and gestational antigens [39–41]. In males, mucin expression within the reproductive tract begins at puberty, corresponding with their period of RORC-Treg colonization [42–44].

Most environments frequented by RORC-Tregs are hypoxic, with hypoxia aiding Th17 T-cells class switching into RORC-Tregs [45]. In the GI tract, typical  $pO_2$  ranges from 15.5 mmHg (resting) to 5.5 mmHg (digesting) [46,47]. The testicular  $pO_2$  is generally near 10 mmHg [48], prostatic  $pO_2$  near 5 mmHg [49], and in the vaginocervical mucosa, the  $pO_2$  is typically 1 mmHg [50–52]. These tissues which host RORC-Tregs are classifiable as hypoxic, defined as  $<15$  mmHg, and indeed more hypoxic than a typical GBM tumor, which generally have a  $pO_2$  near 13 mmHg [53,54].

GBM U87 cells synthesize several steroids from cholesterol, including progesterone, androstenedione and dihydrotestosterone (DHT) [55,56]. Some primary GBM cultures express high levels of CYP17A1, allowing for efficient cholesterol utilization in steroidogenesis [57,58]. In addition to the canonical pathway of steroidogenesis, GBM may also use the ‘backdoor’ route, utilizing aldoketo reductases AKR1C1&3 [59].

The generation of sex steroids by GBM and other cancers initiates expressional changes in both cancer and infiltrating immune cells. Estrogen drives the epithelial to mesenchymal transition in glioma cultures and could act in the same manner in vivo [60]. Androgen receptor is elevated in both men and women’s GBM tumors and blockage of androgen signaling with enzalutamide in vitro leads to a loss of ‘stemness’, causing a reduction in cancer stem cell markers CD133, Nanog and Oct4 [61].

MDSCs and Tregs are antipodally modulated by estrogen and androgen. The *FOXP3* promoter region has an estrogen receptor  $\alpha$  response element that controls expression [62,63], and estrogen suppresses Treg function and proliferation. In con-

trast, estrogen aids MDSC function, potentiated by progesterone [64]. Androgen elevates FOXP3 expression, acting through the androgen response element of the promoter [65,66]. Androgen also dampens the immunosuppressive functionality of MDSCs in vitro and in vivo [67].

We postulated that primary brain cancers, such as GBM, may initiate Treg infiltration by expressing sperm/testicular proteins, such as Glut14, which we have recently demonstrated in GBM primary cultures and in the GBM transcriptome database [68]. If a GBM were to present a sperm/testicular epitope to a reproductive RORC-Treg, then it would begin Treg infiltration and produce an immunosuppressive micro-environment.

Expression of sperm/testicular-specific proteins, some of which have been called cancer/testis antigens, has been observed in many cancer types, including GBM. Analysis of the immunopeptidome of GBM patient serum indicates tumor-derived testicular-, prostate-, placental- and fetal-specific antigens elicit an immune response in these patients regardless of gender [69]. Akiyama and co-workers identified several cancer/testicular antigens expressed by GBM tumors from cultured GBM cells [70], as did Freitas and colleagues [71]. Sreekanthreddy et al. identified pregnancy-specific glycoprotein 9 (PSG9) in GBM patient sera [72]. PSG9, like the other PSGs, activates TGF $\beta$ , which both lures and activates FOXP3<sup>+</sup> Tregs [73], and also drives RORC-Th17<sup>+</sup> cells from a proinflammatory to an immunotolerant form [74].

The sperm/testicular-specific gene *ACRBP* is expressed in GBM in different splice variants [75]. Li and co-workers examined both levels of ACRBP in glioma and the peripheral B-cell response to this protein in glioma patients. ACRBP mRNA transcripts were expressed in glioma and anti-ACRBP antibodies were found in patient sera [76].

The central question we are attempting to address is: what drives the accumulation and activation of immunosuppressive cells into GBM tumors?

We postulated GBMs evade immunosurveillance by two mechanisms. Firstly, they could engage in testicular mimicry, expressing sperm/testicular-specific and testicular-expressed proteins to both draw and activate reproductive Tregs pools keyed toward these sperm/testicular-specific epitopes. Men and women grant immuno-privilege to these epitopes via Tregs to counter immunological shock on the first encounter, and we briefly review this process in Appendix A. Secondly, the GBM tumors could emulate the environment of the placenta, expressing placental immunosuppressive-linked proteins, to provide a niche that attracts MDSCs and immunosuppressive macrophages. For instance, MUC1 is highly expressed in placenta [77], and expression is elevated by both estrogen [78] and progesterone [79]. Additionally, hypoxia elevates MUC1 expression [80], and MUC1 attracts and stimulates immunosuppressive MDSCs [81]. MUC1 is highly overexpressed in GBM and is negatively associated with overall survival [82].

**Markers of hypoxia response, immune cell levels, immune responses, androgen and estrogen reporters.** We have used a gene basket approach of tumor transcriptomes to examine the levels of cell types, status and for reporters of sex steroids. To stratify GBM into the proliferative, mesenchymal, and proneural subclasses, using the method of Teo et al. [83–85], we used the analysis performed by using the Gliovis platform [86].

Reportage of tumor HiF status was calculated from the averaged, normalized levels of hypoxia response genes: Glut1 (*SLC2A1*) [9], Glut3 (*SLC2A3*) [10,11], *ADM* [14], *VLDLR* [13], and *VEGFA* [12].

Reportage of tumor RORC-Treg infiltration was calculated from the averaged, normalized levels of *FOXP3* [23], *CTLA4* [24,87], *GITR* [20,26,88], *RORC* [29,45,89] and *GATA3* [27,90,91].

Reportage of tumor infiltration by microglia [MG] was calculated from the averaged, normalized levels of *ADORA3*, *IGSF6*, *TBXAS1*, *SASH3* and *P2RY13*. Inflammation status was calculated by dividing total MG by averaged, normalized levels of genes downregulated during inflammation, *P2RY12*, *TMEM119* and *GPR34*. Polarization by NF- $\kappa$ B was calculated by dividing averaged, normalized levels of genes known to be upregulated:

*GCLC*, *NQO1*, *GCLM*, *NFKBIA* and *SLC39A8*, with averaged, normalized levels of genes known to be downregulated: *ZDHHC22*, *BCL7A* and *GNG4* [92].

Reportage of tumor infiltration by macrophages was calculated from the averaged, normalized levels of *ITGAM* and *CD68*. Polarization into M1 and M2 states was calculated by dividing total macrophage levels with *ITGAX* [M1] and with *CD163* (M2) transcript levels.

To estimate levels of androgen and estrogen in tumors, we used expression of androgen-controlled *KRT37*, and for estrogen we used the averaged, normalized levels of *THBD* [93,94], *THEMIS2* [95], *SERPINA1* [96], *PIK3CG* [97] and *VAV1* [98], respectively.

## 2. Results

### 2.1. HiF and RORC-Treg Gene Cross Correlation, Tumor Microenvironment and Impacts GBM Patient Outcome

#### Validation of HiF and RORC-Treg Gene Markers

There is a high degree of cross correlation between each of the five genes chosen to report HiF status across the four GBM transcriptome databases utilized.

In Supplemental Figure S1A, we show the cross-correlation plots, correlation coefficients and *p* values (from *t*-tests) of the five genes used for HiF reportage, with data taken from the Agilent (left) and Gravendeel (right) databases, respectively.

In Supplemental Figure S1B, we show the cross-correlation plots, correlation coefficients and *p* values (from *t*-tests) of the five genes we selected for RORC-Treg reportage, with data taken from the Agilent (left) and Gravendeel (right) databases, respectively.

These data clearly indicate that in these two databases, the genes chosen for the HiF and for the RORC-Treg are clearly correlated. Similar statistically significant correlations are found in the CGGA and U133 databases.

As RORC-Tregs of reproductive origin are normally associated with sperm/testicular-specific proteins and found in mucin rich tissues, we examined the cross-correlation plots, correlation coefficients and *p* values (from *t*-tests) of representative RORC-Treg-markers *CTLA4* and *RORC* with sperm/testicular-specific and mucin transcripts, Supplemental Figure S2.

In Supplemental Figure S2, we show that in GBM tumors, the expression of sperm/testicular-specific proteins, *ACRBP*, *SPATA12*, *TSSK6*, *HSPB9*, and *CATSPER1* are highly cross-correlated with each other and with the representative RORC-Treg markers *CTLA4* and *RORC*. A similar pattern emerges when examining the cross-correlations of *CTLA4* and *RORC* with the mucin genes, *MUC5B*, *MUC6*, *MUC13*, *MUC16* and *MUC17*, Supplemental Figure S2B.

Supplemental Figures S1 and S2, drawing on representative datasets Agilent and Gravendeel, show that RORC-Tregs can be present in GBM tumors, and that levels of RORC-Tregs are strongly and significantly correlated with sperm/testicular-specific proteins and mucins.

### 2.2. HiF and Tregs Impacts on Survival and Tumor Microenvironment

We examined the effect of RORC-Treg infiltration in hypoxic and normoxic tumors, by gating transcriptomes for previously described quintets of genes into high/low HiF and RORC-Treg. High/low cuts in each of the gene transcripts were made so as to obtain four roughly sized groups; Treg, Treg&HiF, HiF and neither. This was achieved by utilizing four databases: The Firehose Legacy Agilent microarray (201 patients), the CGGA database (180 patients) [99], the Gravendeel database (122 patients) [100] and the Firehose Legacy U133 platform (389 patients). This stratification methodology allows for assessment of both infiltrating Tregs (a property of the patient's immune response) and tumor HiF status (derived from tumor metabolism and vascularization).

### 2.2.1. Survival and HiF/RORC-Treg Status

Figure 1A shows four Kaplan–Meier survival curves stratified into Treg, Treg&HiF, HiF and neither categories. With each survival curve, the calculated *p* values and median survival (months) are indicated, along with dataset ID. We have omitted markers to identify censored patient endpoints (alive at time of archiving), but these data were used in the statistical analysis.

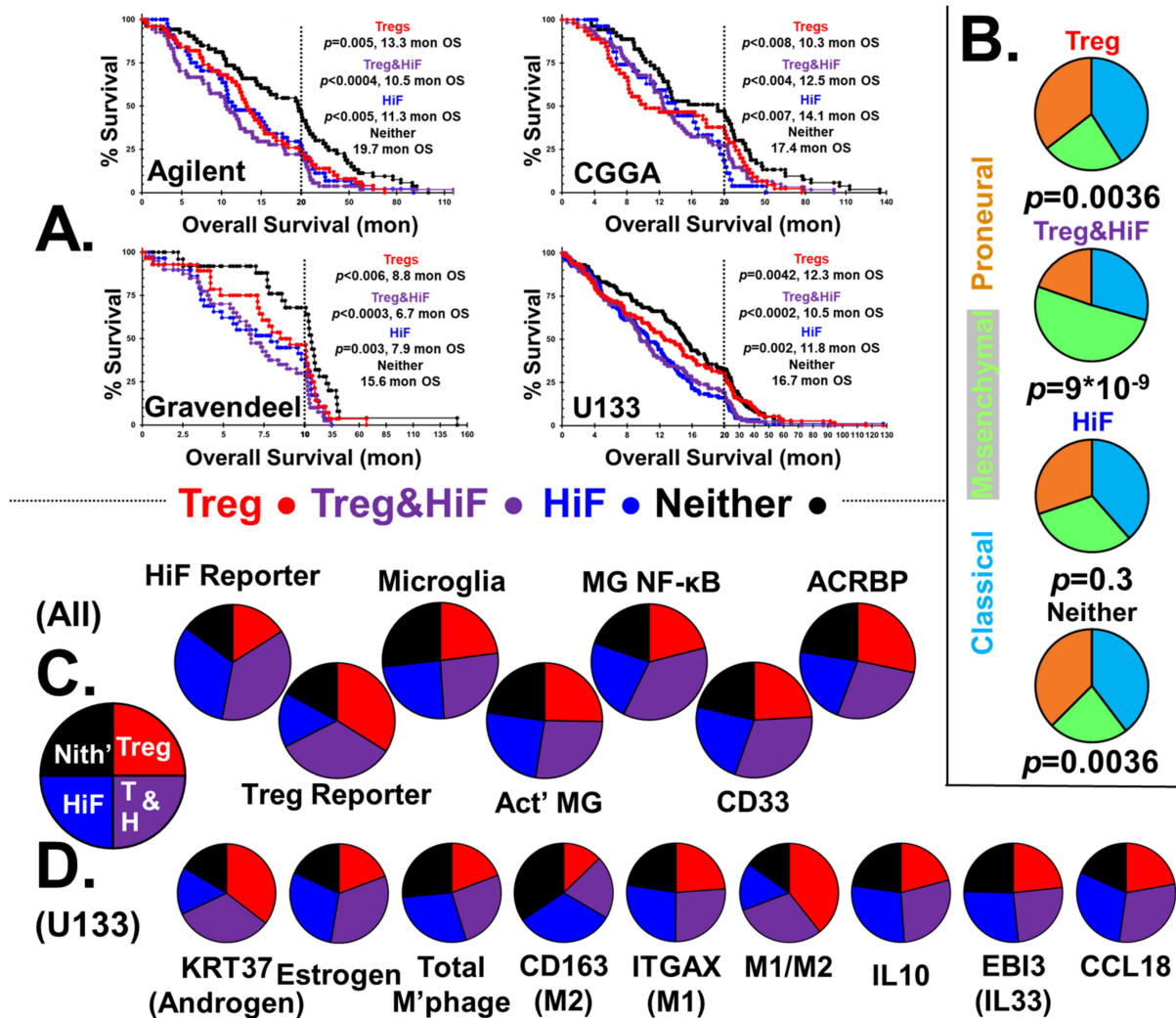


**Figure 1. GBM Patient infiltrating Tregs and HiF Status: Outcome and Characteristics.** (A) Color-coded Kaplan–Meier survival curves of GBM patients stratified for high Treg (red), high HiF (blue), high Treg&HiF (violet), and low Treg&HiF, known as ‘neither’ (black), Agilent, CGGA and Gravendeel and U133 databases. All *p* values are statistically significant,  $p < 0.05$ , when compared to the ‘neither’ group, and median overall survival is indicated in months. (B) The distribution of GBM subtypes in the four stratified groups, compared with the global distribution (37% classical, 32% mesenchymal, and 31% proneural),  $n = 892$ , as pie charts. Pie charts are color-coded with classical (light blue), mesenchymal (light green) and proneural (burnt orange). *p* values calculated from utilizing the  $\chi^2$ -test are shown. (C) Pie charts indicating seven markers of interest,  $n = 892$ , from normalized transcripts reporting medians. From left to right; HiF and Treg gene baskets validate stratification methodology. Total microglia (MG) are highest in normoxic tumors without Tregs, whereas both inflammation and NF-κB activation markers are elevated in HiF tumors. Myeloid cell marker *CD33* is elevated in hypoxic tumors. *ACRBP*, which cross-correlates with other sperm/testicular-specific proteins, correlates with RORC-Treg infiltration.  $p < 0.05$  in all cases utilizing *t*-tests. (D) Data from U133 database, examining sex steroid and macrophage phenotypes in stratified groups in the form of pie charts. Androgen reportage (*KRT37* transcript levels) associates with RORC-Tregs, whereas hypoxia correlates with estrogen reportage. Macrophage infiltration (*ITGAM* and *CD68*) tracks hypoxia, and M2/M1 polarization markers *CD163* and *ITGAX* indicate RORC-Tregs appear to drive M1 > M2. *IL10*, *EBI3* and *CCL18* levels are biased toward hypoxic tumors.  $p < 0.02$  in all cases utilizing *t*-tests. Individual *t*-test results in Supplemental Table S1.

Patients whose tumors have infiltrating RORC-Treg or the HiF phenotype have a significantly worse outcome than normoxic and non-Treg-infiltrated tumors. Patients with Warburg phenotype tumors highly infiltrated by Tregs generally tend to have the worst outcome, with median survival <50% of the neither group.

We analyzed the reportage levels of HiF and RORC-treg gene baskets from all patients in the four databases,  $n = 892$ . Stratification by HiF/Treg results in the median HiF gene-basket reportage at levels  $2.4 \pm 0.7$  times greater in the selected HiF subgroups than normoxic subgroups. The median RORC-Treg gene basket is expressed at levels  $2.3 \pm 0.9$  times greater in the selected Treg subgroups than the negative pair; calculated  $p$ -values are  $p < 10^{-10}$  between pairs in both cases.

### 2.2.2. CMP Subtypes

The distribution of CMP-subtypes in the stratified tumors are shown in Figure 1B, along with  $\chi^2$  calculated  $p$ -values. In the hypoxic-Treg infiltrated tumors, the mesenchymal subtype dominates, in contrast to the normoxic-Treg infiltrated tumors with elevated classical and proneural sub-types.

### 2.2.3. Stratification Reportage and Microglial Phenotypes

Levels of HiF and RORC-Treg markers of the four stratified groups are displayed in Figure 1C, using pie charts derived from 892 patients (U133, Aglient, Gravendeel and CGGA datasets). Total microglia levels were elevated in the neither subgroup, the only immunological cell type correlated with improved patient outcome,  $p < 0.01$ , Figure 1C. Poor patient outcome is correlated with microglia activation state with both proinflammatory and elevated NF- $\kappa$ B signaling over-represented in the at-risk subgroups.

### 2.2.4. MDSCs

CD33 expression is a proxy for MDSC levels [101], and levels are overrepresented in hypoxic tumors, potentiated by RORC-Treg infiltration.

### 2.2.5. Sperm/Testicular Proteins

Li and coworkers found antibodies toward sperm-specific protein ACRBP in the serum of their glioma patients [76]. We chose to examine *ACRBP* as a representative of sperm-specific gene expression in GBM tumors (see Supplemental Figure S2A). Expression of *ACRBP* is concordant with degree of Treg infiltration, but independent of HiF status, as shown in Figure 1C.

### 2.2.6. Androgen and Estrogen Reporters and Macrophage Status

The expression of *KRT37* is controlled by three androgen response elements, and transcript levels can serve as an androgen/androgen receptor signaling proxy [102–105]. GBM tumor levels of *KRT37* are highly correlated with Treg infiltration. Supplemental Figure S3 shows the correlations between expression of *KRT37* (i.e., androgen expression) and the RORC-Treg gene basket, using the U133 dataset. Individual RORC-Treg markers are highly correlated with *KRT37*, all correlations  $p < 0.001$ , suggesting androgen-driven expansion and activation of Treg populations in GBM tumors [66]. In Figure 1D, we show pie charts representing the sex-steroid reporter levels and macrophage status using the U133 dataset. Using *KRT37* androgen reportage, it is clear that there is a strong correlation between androgen reportage and RORC-Tregs.

Our estrogen reporter is generated from a basket of normalized transcripts utilizing the quintet of estrogen-responsive genes: *THBD* [93,94], *THEMIS2* [95], *SERPINA1* [96], *PIK3CG* [97] and *VAV1* [98]. These gene expression levels are highly correlated, Supplemental Figure S4, with all correlations  $p < 0.001$ . In Figure 1D, it is clear that estrogen reportage correlates with HiF status.

We calculated total macrophages levels using normalized levels of classical markers *ITGAM* and *CD68*. Hypoxia has been shown to aid macrophage recruitment and

polarization toward the M2-phenotype [106], which is what we observe. The M2 > M1 hypoxic tumors are also noteworthy in their expression of anti-inflammatory, macrophage-associated, cytokine/chemokines IL10, EBI3 (co-protein in IL33) and CCL18.

In pursuit of a mechanistic explanation for immune responses in the subgroups, we examined the correlation of stratified subtypes with > 2200 genes. Figure 2 shows selected genes found highly expressed in the Treg, Treg&HiF and HiF subtypes (using the U133 dataset),  $p < 0.05$ .

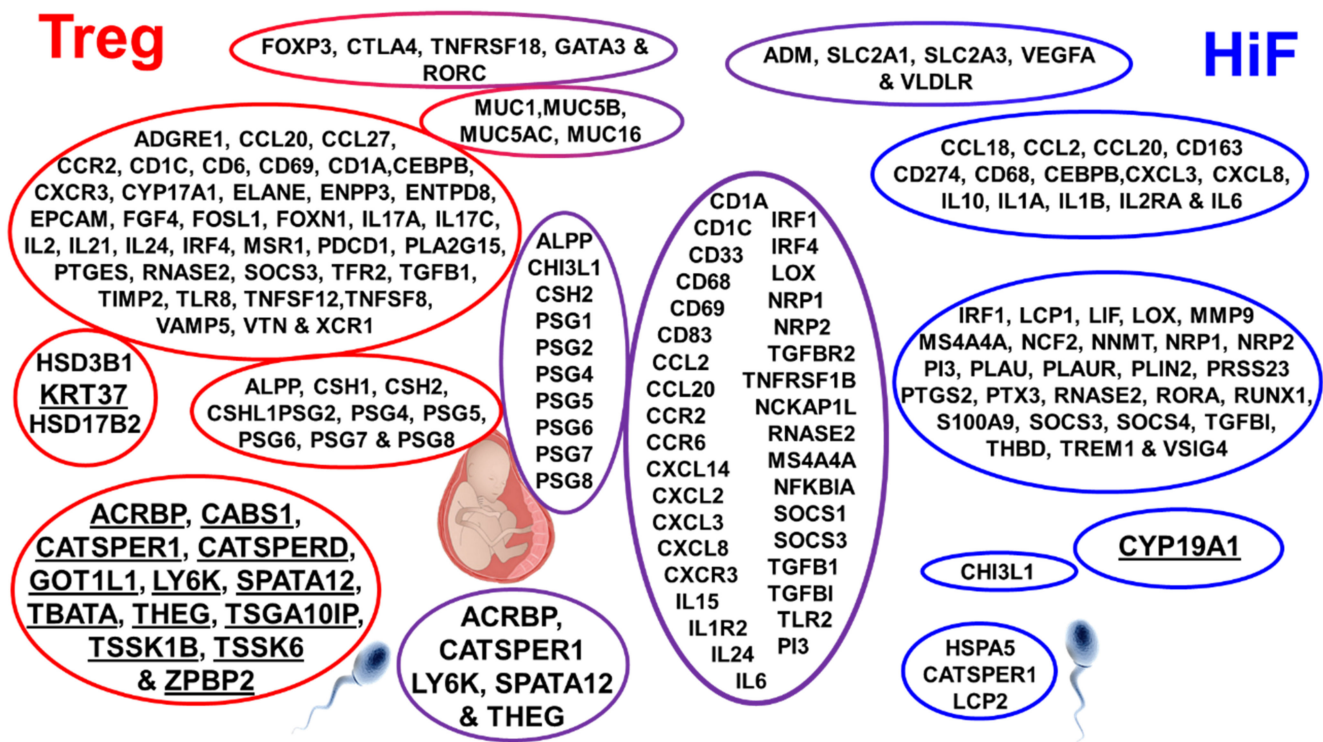


**Figure 2. Genes correlated with Treg and HiF clusters:** the breakdown of gene expression by high Treg expression subtype (left), high HiF expression subtype (right), and high Treg and HiF expression (middle). Genes clustered and highlighted are sperm/testicular proteins, including *ACRBP* and gestational genes such as PSGs. The androgen-responsive gene *KRT37* is associated with Tregs, as are many reproduction-associated genes, including sperm-specific, placental-associated and mucins genes. In contrast, aromatase (*CYP19A1*), which converts testosterone to estrogen, is associated with hypoxia. Noteworthy too is the HiF association with immunosuppressive M2 macrophage markers, including *CD68*, *CD69*, *CD163*, *MS4A4A*, and MDSC inducer *MUC1*. We also observe M2 macrophage cytokines *CCL2* and *CCL13* and *IL10* which can give rise to this polarization in hypoxic GBM.

The genes are clustered into groups based on cell type and function. The Treg subtype is to the left, HiF is on the right and Treg&HiF is centered, Figure 2. Bolded for emphasis are:

- Keratin 37, our androgen reporter, correlates with Tregs.
- Aromatase (*CYP19A1*), which converts testosterone to estrogen is elevated with HiF.
- Sperm/testicular-specific gene transcripts *ACRBP*, *CATSPER1*, *LY6K*, *SPATA12* and *THEG* all correlate with Tregs.

### 2.3. Steroidogenic Status Impacts GBM Patient Outcome

#### 2.3.1. Steroidogenesis in GMB

An examination of steroidogenic enzyme gene levels in the stratified GBM tumors, Figures 1 and 2, indicated that there were two pathways for steroidogenesis in GBM tumors: the canonical and 'backdoor' pathways. Based on this emergent property, we stratified the tumors from the four databases based on the expression of enzymes required for steroido-

genesis. GBMs were first stratified by  $\approx 50\%$  based on the high expression of canonical steroidogenic pathway genes. Those with the canonical pathway were then subdivided, based on aromatase expression, into androgen- (with progesterone) and estrogen (with progesterone)-generating tumors. The remaining GBMs with low levels of the enzymes of the canonical pathway were then stratified into two equally sized fractions of those expressing the non-canonical ‘backdoor’ pathway genes, which generated dihydrotestosterone and estrogen, and the tumors which appear to be asteroidogenic (See Methods).

### 2.3.2. Overall Survival and Status

Figure 3A shows the Kaplan–Meier survival curves of GBM patients stratified into steroidogenic phenotypes; androgen and progesterone, with low estrogen (A&P), estrogen and progesterone, with low androgen (E&P), estrogen and androgen, low progesterone (E&A), and asteroidogenic groups. Also shown is the median survival in months and the calculated  $p$  values with respect to the asteroidogenic group. Markers identifying censored patient endpoints were again omitted but used in statistical analysis. GBM steroidogenesis is highly detrimental to patient outcome, with median survival time of the E&A group only 75% that of the asteroidogenic group. Patients with A&P/E&P tumors fare worse, with only  $\approx 60\%$  of the longevity of the low steroid group.

### 2.3.3. CMP Subtypes

In Figure 3B, we show the distribution of CMP subgroups, stratified by steroidogenic output, capturing the role of sex steroids in GBM etiology. Levels of mesenchymal cells in the three steroidal groups are consistent with reported effects of sex steroids on epithelial–mesenchymal transition. Reports state progesterone fetters the epithelial–mesenchymal transition [107], whereas androgen’s effects are much weaker [108]. In contrast, estrogen was shown to drive the epithelial–mesenchymal transition in many tissues, including GBM cells [60]. We find estrogen causes over-representation of mesenchymal phenotype GBMs, whereas progesterone favors the classical CMP subgroup.

### 2.3.4. HiF and Tregs

The first two pie charts of Figure 3C show there is a small, statistically significant elevation in HiF reportage in tumors with the ability to generate androgen and estrogen,  $p < 0.05$ . Androgenic GBMs clearly show elevated levels of infiltrating RORC-Tregs,  $p < 0.001$ .

### 2.3.5. Microglial Phenotypes

The two estrogenic subtypes induce microglial proliferation and have elevated NF- $\kappa$ B activation markers, which matches studies performed in vitro and in vivo [109,110]. In contrast, both progesterone and androgen suppress NF- $\kappa$ B pathway activation with progesterone acting directly through its receptor, but with androgen indirectly acting via cytokine signaling [111,112].

Microglia infiltration is elevated in estrogenic GBM, with levels elevated  $>40\%$ ,  $p < 0.001$ , and we observe  $>30\%$  NF- $\kappa$ B signaling in estrogenic GBM,  $p < 0.001$ , Figure 3C. Unlike combinatorial estrogen and progesterone, combined androgen and progesterone has a synergistic effect on microglia NF- $\kappa$ B signaling, with the difference between A&P and E&P groups being 3:1,  $p < 0.001$ .

### 2.3.6. MDSCs

GBM tumor infiltration by MDSCs is estrogen sensitive, with marker *CD33* overrepresented,  $p < 0.001$ , Figure 3C [113,114]. Elevated expression of the estrogen signaling reporter basket of genes correlates with MDSC and TAM marker genes [115], Supplemental Figure S5, all correlations  $p < 0.001$ . This is consistent with our postulate that GBMs are steroidogenic, allowing the tumors to mimic reproductive tissues that attract either RORC-Tregs or MDSCs/TAMs.

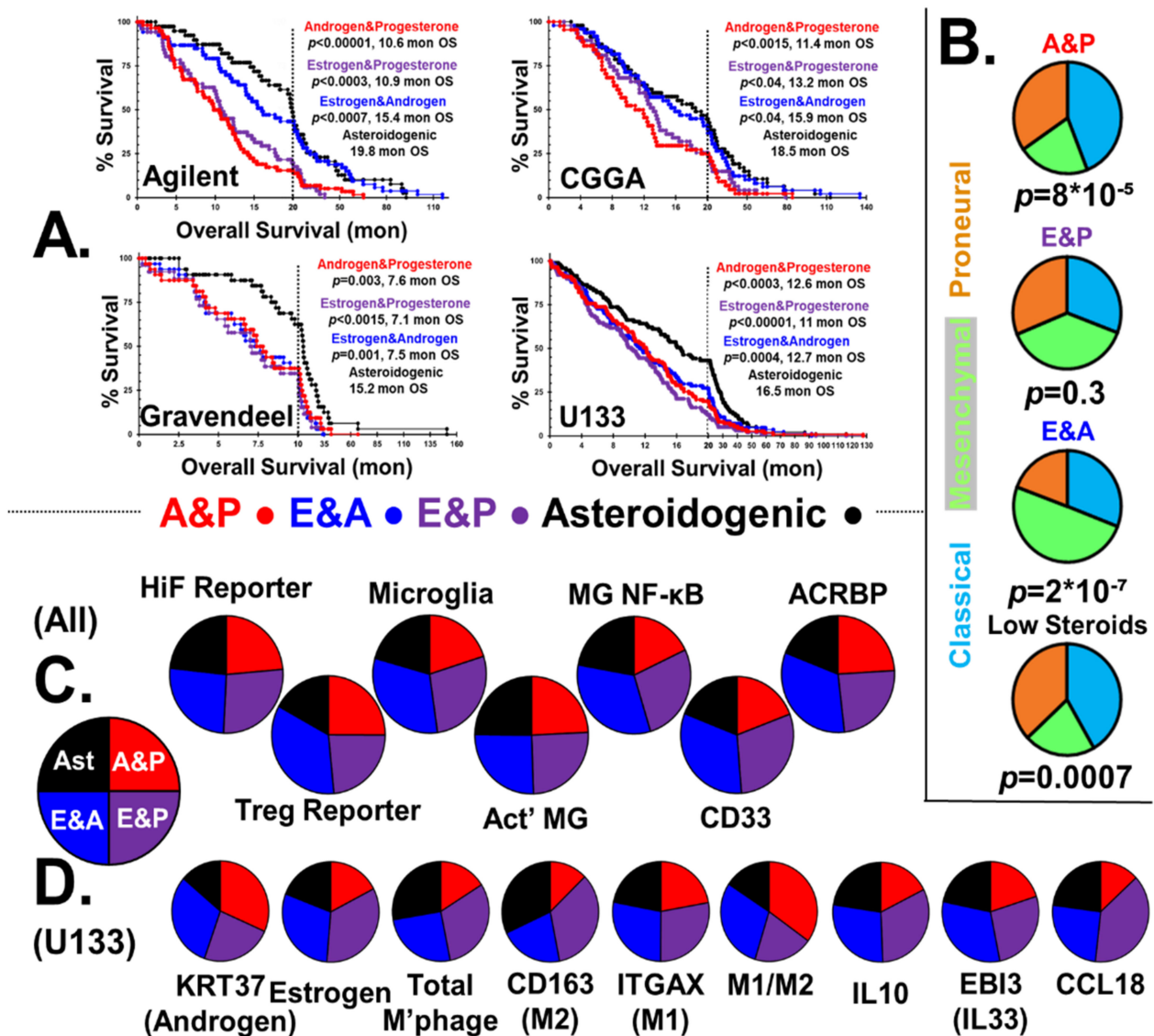


**Figure 3.** GBM Patient Sex Steroid synthesis: Outcome and Characteristics. (A) Kaplan–Meier survival curves of GBM patients with tumors stratified by high androgen/progesterone; low estrogen (red), high estrogen/progesterone; low androgen (violet), high estrogen/androgen production; low progesterone (blue), and overall low steroid production, asteroidogenic (black). All *p*-values are statistically significant compared to the low group. (B) CMP subtypes of GBMs correlate with androgen, estrogen and progesterone expression. (C) Data from all four databases in the form of pie charts indicating the amount of steroidal influence on seven markers of interest, all statistically significant at *p* < 0.05 except microglial activation. Estrogenic GBMs have elevated HiF and androgenic GBMs have infiltrating RORC-Treg reporter levels. Estrogenic GBMs are associated with microglial infiltration and NF-κB signaling. Myeloid cell infiltration reporter CD33 tracks estrogen, with a 2:1 ratio of CD33 levels in estrogenic tumors compared with tumors with low estrogen. Sperm-specific ACRBP clearly correlates with androgenic GBM subtypes. (D) U133 database pie charts indicating that androgen and estrogen reporter genes track the steroidogenic stratification. Total macrophage levels are low in androgen and progesterone. Sex steroids clearly affect the M2/M1 polarization, with androgen driving M1 > M2, but estrogen driving M2 > M1. Levels of immunosuppressive IL10 and CCL18 correlate with estrogen, but EIB3 generation is inhibited by androgen. *p* < 0.02 in all cases utilizing *t*-tests. Individual *t*-test results are in Supplemental Table S2.

### 2.3.7. Sperm/Testicular Proteins

Expression of ACRBP is concordant with the degree of steroidogenesis, Figure 3C. Expression of ACRBP is strong in all three sex-steroid groups, all statistically significantly different from the asteroidogenic group, *p* < 0.001, but the two androgenic types are indistinguishable from each other. This observation supports the postulate that sperm-

specific proteins are expressed by GBM to lure testicular/uterocervical Treg pools. From an analysis of the relative levels of different steroidogenic enzyme transcript levels, we present the routes and relative fluxes of steroidogenesis for the A&P, E&P and E&A groups in Supplemental Figure S6. Additionally, the ability to block steroidogenesis with off-the-shelf clinical inhibitors is shown.

#### 2.3.8. GBM Steroidogenesis Validation, Macrophage Infiltration and Polarization

Estrogen acts as a potent anti-inflammatory regulator in healing and causes macrophage polarization M2 > M1 [116]. Progesterone acts in a similar manner to estrogen, driving M2 > M1 polarization [117]. The E&P group has the highest fraction of both total macrophages and M2-polarized macrophages. Androgens can initially aid M2 > M1 polarization; however, prolonged androgen exposure has been shown to cause M1 > M2 macrophage polarization [118], consistent with our stratification of GBM by steroidogenesis. Macrophage levels and polarization in the four types of tumors is consistent with the reported estrogen anti-inflammatory M2-phenotype, driving also the production of IL10 and IL33, but androgen driving M2 > M1 polarization. CCL18 generation by M2 macrophages is elevated by estrogen [119], and our data suggest that it is inhibited by androgen.

#### 2.4. Elevation of Sperm/Testicular Specific Antibodies in GBM Patients

Emboldened by this *in silico* data, we reasoned that GBMs shed sperm/testicular-specific proteins into the peripheral lymphatic system. In adults, the levels of anti-sperm/testicular antibodies in circulation are very low, as reactive B-cell lineages are either deleted or converted into Bregs, either in testicles or by the seminized cervix (Appendix A). Shed sperm/testicular-specific antigens from a GBM tumor should generate anti-sperm/testicular-specific antibodies in patient serum. It has been demonstrated that following vasectomy or vaccination, sperm introduced in the periphery induce an immune response, and so high titers of anti-sperm antibodies develop [120–125]. Men, following vasectomy, have elevated circulating anti-sperm antibodies, but do not suffer from autoimmune orchitis because testicular immune privilege is maintained by Tregs [120–122,126].

We devised a methodology to interrogate GBM patient serum for multiple anti-sperm/testicular antibodies, whereby we labeled human antibodies with specificity toward proteins present in primate testicle slices. We used primate testicle as sperm-specific proteins generally have very high rates of evolution due to sperm competition, especially in small mammals [127]. This testicular tissue was obtained from control animals from a different study that had come to an end, and we were able to obtain and fix the tissue within minutes of euthanasia.

We incubated monkey testicular slices with serum from GBM patients and age-matched controls. Then, we labeled the tissue for the presence of human IgG. As a privileged organ, anti-sperm/testicular antibody binding to the monkey testicle should be low in both women and in unvasectomized men.

Figure 4 shows that the levels of anti-testicular antibodies were elevated in GBM patients compared with gallbladder surgery patients. In Figure 4A, we show a plot comparing the intensity of DAB-staining intensity in anti-sperm/testicular antibodies binding to monkey testicular tissue. We find nearly sevenfold greater levels of anti-sperm/testicular antibodies in GBM patient serum compared to control serum,  $p < 10^{-10}$ .

Figure 4B,C allows the comparison of DAB (brown) labeling of monkey testicle with anti-sperm/testicular antibodies from the serum from two male and two female gallbladder surgery patients (B) and that from the serum of four male and four female GBM patients (C). The nuclei counter-stained blue.

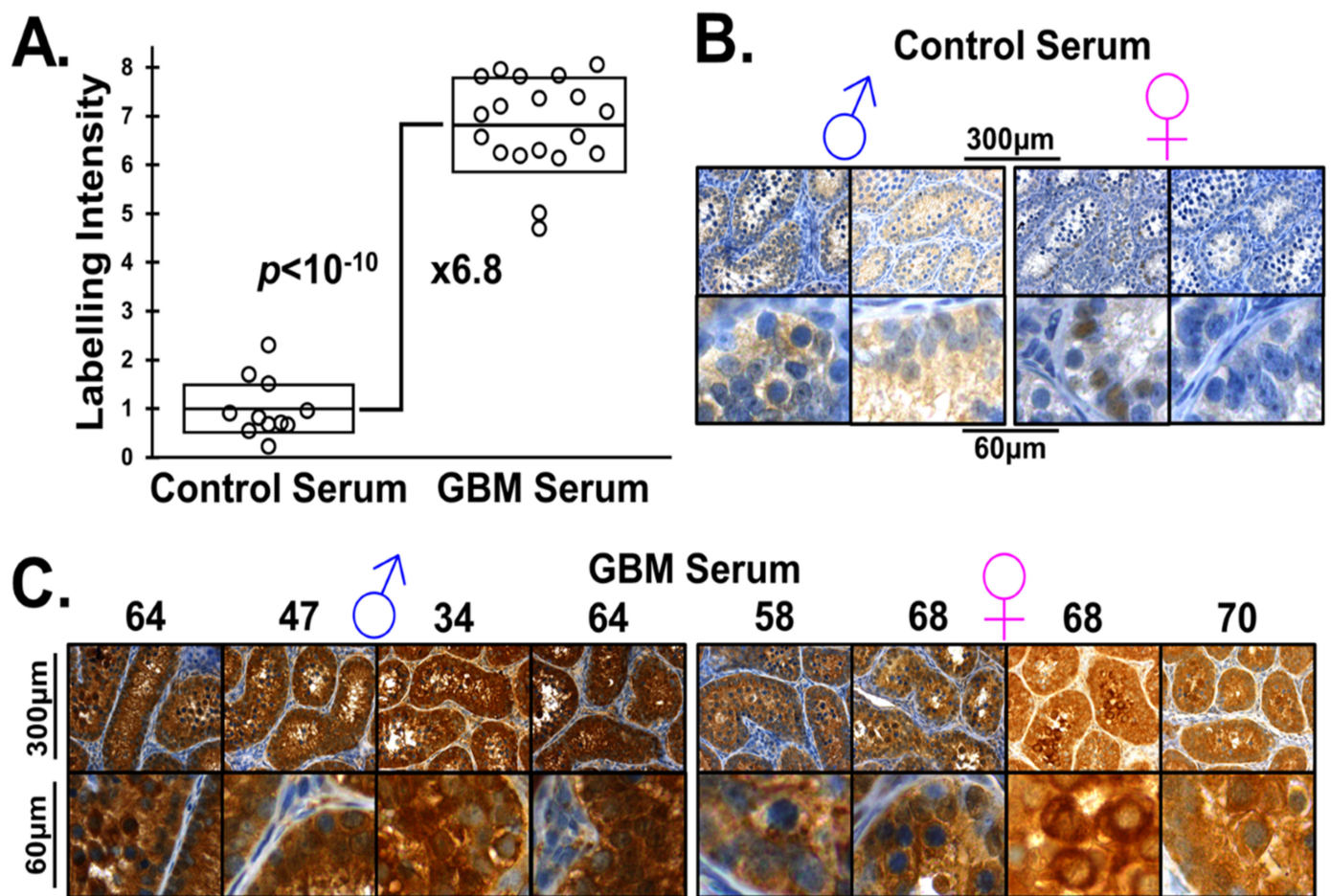


**Figure 4. Monkey Testicle labeled with Patient Serum.** (A) Staining intensity is significantly greater in the GBM than the control serum when brightness is quantified and scaled, nearly sevenfold that of the control, mean and SD boxed,  $p < 10^{-10}$ . (B) Labeling of Cynomolgus monkey testicle using serum from control patients. Low levels of anti-sperm/testicular antibodies, and therefore light staining can be observed. (C) The significant staining on Cynomolgus monkey testicle when treated with patient sera indicates the presence of antibodies to testicular germ cells and to sperm at all stages of development. Patient age is atop the images.

The images in Figure 4B,C clearly show a heterogeneous pattern of patient-derived antibody testicular labeling, which can be seen in the high magnification images, suggesting that different testicular epitopes are targeted/labeled in each patient's serum. These antibodies arise from differential sperm/testicular-specific proteins expressed by an individual patient's GBM, recruiting a separate pool of reproductive Tregs. The labeling of testicular slices with serum samples taken from other GBM and control patients are shown in Supplemental Figure S7. We conclude two things: first, sperm/testicular-specific IgGs are present in GBM patient serum, and second, these antibodies arise due to sperm/testicular-specific proteins being expressed by the tumors.

### 3. Discussion

We have used a gene-basket approach to stratify GBM tumor transcriptomes, which has been used to examine the levels of specific cell types and signaling/synthetic pathways in tumors. A drawback of this type of analysis is that although we can identify correlations between gene transcripts, we cannot be sure that the transcripts are present in the same cells. The tumor-infiltrating RORC-Tregs we have shown to be linked to poor patient outcomes and associated with tumor androgenesis were selected based on elevated levels of *FOXP3*, *CTLA4*, *GITR*, *RORC* and *GATA3* transcripts in the whole tumor, not from individual T-cells. A reasonable criticism of the in silico analysis performed is that these transcripts could be

expressed by different cells within the tumor, and the correlations between the transcripts are spurious, in the same manner that rates of forest fires and ice-cream sales are spuriously correlated. With respect to the identification of tumor-infiltrating RORC-Tregs, additional evidence for this supposition is that the relationship between levels of the identified infiltrating RORC-Tregs and patient outcome is consistent utilizing data drawn from four different GBM transcriptome databases. Additionally, these RORC-Tregs transcripts are not only highly cross-correlated with each other, but also highly correlated with transcripts known to be recruiters of this Treg subclass, 'male-specific' *ACRBP*, *SPATA12*, *TSSK6*, *HSPB9* and *CATSPER1*, and with mucins *MUC5B*, *MUC6*, *MUC13*, *MUC16* and *MUC17*.

Our *in silico* analysis identified tumor steroidogenesis as a means for GBM to acquire an immunosuppressive phenotype, with the generation of androgens appearing to drive RORC-Treg infiltration and the generation of estrogen driving infiltration/activation of MDSCs/TAMs. Steroidogenesis can either be supported by the GBM cells, from non-cancer cells within the tumor, or an interplay between both. It has recently been reported that tumors can cause the expression of *CYP11A1* in T-cells, causing them to metabolize cholesterol to pregnenolone. This hormone is then released, resulting in immunosuppression [128]. The stratification of GBM tumors based on the synthesis of androgen and estrogen can be, and has been, validated by monitoring the transcripts of androgen-dependent (*KRT37*) and estrogen-dependent (*THBD*, *THEMIS2*, *SERPINA1*, *PIK3CG* and *VAV1*) reporter transcripts. We have presented a multiplicity of evidence for the generation of androgens by GBM tumors to be correlated with levels of RORC-Tregs, and for estrogen synthesis by these tumors to correlate with infiltration by immunosuppressive MDSCs and macrophages.

In GBM patients, we observe compartmentalization between an immune-privileged tumor microenvironment and a peripheral immune response, evident from the >6-fold increase in circulating anti-sperm/testicular antibodies. A similar discordant immune response is observed post-vasectomy. Vasectomy does not cause autoimmune orchitis, but the release of 'male-specific' proteins into the periphery causes elevated anti-sperm antibodies. Testicular Tregs maintain immune privilege following vasectomy, despite a peripheral immune response. This same immune compartmentalization appears to occur in GBM patients.

The heterogenous pattern of patient-derived antibody testicular labeling, which can be seen in the high magnification images, suggests different testicular epitopes are targeted/labeled in each patient's serum. These antibodies arise from differential sperm/testicular-specific proteins expressed by an individual patients' GBM tumors, recruiting a separate pool of reproductive Tregs. The reproductive Treg populations must be lured into the tumor microenvironment to become activated toward male-specific epitopes, and one of the most promising candidates is the mucins expressed by GBM. *MUC16* has previously been shown to generate a Treg-attracting fragment after proteolysis, which has previously been shown to result in tumor aggressiveness in ovarian cancers [38].

#### 4. Materials and Methods

The *in silico* transcriptome analysis we report is derived from four publicly available datasets using only IDH wild-type GBM tumors: the Firehose Legacy U133 (389 patients), the Firehose Legacy Agilent microarray (201 patients), the CGGA [99] database (180 patients) and the Gravendeel [100] database (122 patients). The classification of GBM sub-types refined by Wang et al. was taken from the analysis furnished by the Gliovis platform [86].

##### 4.1. Stratification of GBM Phenotype by Warburg and Treg Infiltration Status

###### 4.1.1. Stratification of GBM Tumors by HiF

We used a basket approach to stratify tumors into positive/negative HiF based on expression of the hypoxia-response genes: *Glut1 (SLC2A1)* [9], *Glut3 (SLC2A3)* [10,11], *ADM* [14], *VLDLR* [13] and *VEGFA* [12]. Normalized mRNA expression levels of the five

genes were rescaled between 0 (min) and 1 (max) and then averaged. The 5–10% fraction of tumors expressing low levels of each marker were relegated into HiF negative status, and the  $\approx 50\%$  tumors displaying the highest average expression were deemed as HiF positive. GBM tumor expression of HIF signature gene cross-correlations is shown in Supplemental Figure S1 using data obtained from the Firehose Legacy Agilent microarray [129] and the Gravendeel databases [100] with plots generated utilizing Gliovis [86]. *SLC2A1*, *SLC2A3*, *ADM*, *VLDLR* and *VEGFA* expression levels in GBM populations are highly cross-correlated with the other HiF markers, with  $p < 0.001$  in all cases. To identify HiF status, we normalized and rescaled the expression levels of the quintet; the 5–10% fraction of tumors expressing low levels of each marker were deemed HiF negative; the  $\approx 50\%$  tumors displaying the highest average expression were deemed as HiF positive.

#### 4.1.2. Stratification of GBM Tumors by Tregs

After the transcriptome data had been stratified into two similar groups representing hypoxic and normoxic, it was once more re-stratified. In the second round of stratification, the samples were divided on the basis of high/low levels of RORC-Treg markers. The GBM-infiltrating RORC-Tregs were selected on the basis of elevated expression of a 5-gene signature; *FOXP3* [23], *CTLA4* [24,87], *GITR* [20,26,88], *RORC* [29,45,89] and *GATA3* [27,90,91]. The cross-correlations of GBM tumor expression of these Treg signature genes is shown in Supplemental Figure S2, with data obtained from the Firehose Legacy Agilent microarray and Gravendeel GBM tumor databases [100,129] and plots generated using the Gliovis platform [86]. The quintet of genes used to identify tumor infiltrating Tregs are highly cross-correlated with the other, with  $p < 0.001$  in all cases.

To identify RORC-Treg high/low status, we normalized and rescaled the expression levels of the quintet; the 5–10% fraction of tumors expressing low levels of each marker were deemed RORC-Treg low, and the  $\approx 50\%$  tumors displaying the highest average expression were deemed as Treg high.

#### 4.1.3. Selection of Treg&HiF and Neither Groups

After assignment of HiF and Treg status, the data fell into four distinct groups: high Treg, high HiF, high Treg&HiF, and 'neither' (low Treg and low HiF). The mRNA levels of highlighted gene expression levels with respect to the neither group is found in Supplemental Table S1A (Excel Sheet, Treg&HiF Stratification), along with the fractional size of the four groups, for analysis from the four presented databases. The normalized average HiFs are  $2.4 \pm 0.7$  times greater in the HiF-positive groups than in the HiF-negative groups and the Treg groups are  $2.3 \pm 0.9$  times greater in the Treg high groups than in the Treg low groups across the four databases.

#### 4.1.4. Assaying Microglia Levels and Status

Given that microglia exhibit sex-specific phenotypes (Yanguas-Casás [130]), these immune cells were a major target of investigation. Tumor-infiltrating microglia and their inflammatory status were interrogated using the gene expression of 4 separate baskets, averaging the products of normalized/rescaled mRNA expression levels of each gene in a basket, with baskets drawn from transcriptome changes induced by LPS treatment or stimulation of NF- $\kappa$ B signaling in human microglial cultures (total MG: *ADORA3*, *IGSF6*, *TBXAS1*, *SASH3* and *P2RY13*; downregulated during inflammation, *P2RY12*, *TMEM119* and *GPR34*; upregulated by NF- $\kappa$ B: *GCLC*, *NQO1*, *GCLM*, *NFKBIA* and *SLC39A8*; and downregulated by NF- $\kappa$ B: *ZDHHC22*, *BCL7A* and *GNG4*) [92].

### 4.2. Stratification of GBM Phenotype by Steroidogenesis

#### 4.2.1. Choice of Genes for Stratification of Tumors by Steroidogenesis

We initially analyzed GBMs based on the genes of the canonical steroidogenesis pathway and planned to divide GBM tumors into androgenic, estrogenic and asteroidogenic groups. However, upon examining the outputs of androgen and estrogen reporter genes, it

was evident that some GBMs had low transcript levels of critical canonical steroidogenic pathway genes, and yet appeared to be generating androgen and estrogen. This emergent property of the tumors led us to examine the non-canonic ‘backdoor’ steroidogenic pathway, which is utilized during gestation and in castration-resistant prostate cancers. We discovered that in some GBMs, this non-canonical pathway appears to be present, and so we used a stratification procedure that gave rise to four steroidogenic phenotypes: androgen (testosterone) with progesterone (A&P), estrogen with progesterone (E&P), estrogen with androgen (DHT) (E&A), and asteroidogenic.

#### 4.2.2. Canonical Steroidogenesis Groups A&P and E&P

The A&P and E&P subgroups use the canonical steroidogenesis pathways, expressing high levels of canonical pathway genes *CYP11A1*, *CYP17A1*, *HSD17B3* and *HSD3B1* alongside low levels of the progesterone catabolic enzyme *AKR1C1*. We selected the  $\approx 50\%$  of tumors with high levels of the first four genes and low *AKR1C1*. These were then stratified based on expression of aromatase (*CYP19A1*), which converts testosterone into estrogen, delineating the A&P and the E&P subtypes.

#### 4.2.3. Non-Canonical Steroidogenesis, the E&A Group

Approximately a quarter of the GBM tumors appear to employ non-canonic steroidogenesis, similar to estrogen-sensitive breast cancers [131,132] and castration-resistant prostate cancers [55,133–136]. Instead of beginning with cholesterol, steroid-sulfates are utilized, imported by fetal/placental transporters *SLC22A11*, *SLC22A19*, and *SLCO4A1*: the ‘side-entry’ synthetic route. These GBM then utilize *AKR1C1* and *AKR1C3* for ‘backdoor’ steroidogenesis [131,134,135,137–140]. Tumors lacking this non-canonical importation (asteroidogenic) were identified by low levels of all five gene transcripts.

#### 4.2.4. Selection of Androgen/Estrogen in the Four Groups

An emergent property was apparent during an initial analysis of the steroidogenic enzyme/transporter gene levels, indicating that GBM can be stratified into 4 groups: A&P (testosterone and progesterone), E&P (estrogen and progesterone), E&A (Estrogen and dihydrotestosterone), and ‘neither’ (asteroidogenic). The mRNA levels with respect to the neither group are found in Supplemental Table S1B (Excel Sheet, Sex-Steroid Stratification), along with the fractional size of the four groups for each of the four databases analyzed. Normalized average androgen reportage is  $2.4 \pm 0.7$  times greater for two androgen-positive groups than in the asteroidogenic group, and estrogen reportage in the two estrogen groups is  $2.0 \pm 0.6$  times greater than the asteroidogenic group.

#### 4.2.5. Visualization of Anti-Sperm Antibodies from Patient Sera

Unless otherwise stated, reagents were obtained from Sigma (Sigma-Aldrich, Inc., St. Louis, MO, USA). We probed primate testicle with patient serum, then visualized human antibodies with DAB staining. At necropsy, Cynomolgus monkey testicle was removed and fixed in 4% paraformaldehyde buffer for 7 days at 4 °C. The tissue was then washed and dehydrated using graded alcohol and xylene and then wax embedded. The block was sliced into 5  $\mu\text{m}$  sections that were affixed to slides and dried. Slides were dewaxed four times in xylene, then twice in isopropanol, and rehydrated using graded ethanol. The slides were washed and permeabilized using Phosphate Buffered Saline (PBS, Fisher Scientific, Waltham, MA, USA) containing 0.1% Triton X-100. The slides were placed in Na-citrate buffer (100 mM, pH 6.0) and heated to  $<100$  °C in a steamer for 30 min, followed by cooling slowly to bench temperature for epitope retrieval. After washing in PBS, endogenous peroxidase activity was eliminated using mild conditions: 1.8%  $\text{H}_2\text{O}_2$  for 5 min, then in 1% sodium periodate for 5 min, followed by 0.02%  $\text{NaBH}_4$  for 2 min. Serum-Free Protein Block (Dako North America, Inc., Carpinteria, CA, USA) was applied for 1 h, and after washing, 50  $\mu\text{L}$  of GBM or gallbladder surgery patient serum was applied and incubated at 4 °C overnight. After washing in PBS, 1:500 mouse anti-human

IgG antibody (HP-6017) was applied and incubated for four hours. After washing, the HiDef™ HRP-polymer system (Cell Marque, Rocklin, CA, USA) was used to functionalize with peroxidase, and a DAB chromogen kit (Dako North America, Inc., Carpinteria, CA, USA) was used for visualization. Slices were then counter-stained using hematoxylin and sealed. Images were taken with a Carl Zeiss microscope (Oberkochen, Germany), and DAB labeling levels were quantified using ImageJ, as previously described [141,142]. We used an age-matched control group, as anti-sperm antibody titers have a slight age dependency [120,121]. Gallbladder surgery patient serum was used for control studies as these are demographically akin to GBM patients, and these samples were obtained from the Houston Methodist Biorepository. Anti-testicular antibodies were assayed using serum from GBM patients (10♀, 12♂) and gallbladder surgery controls (5♀, 6♂). All samples were treated simultaneously, in parallel, at each step of the immunohistochemistry process, incubated for the same time and using the same solutions.

## 5. Conclusions

Tumor hypoxia and infiltration by Tregs and also by CD33<sup>+</sup> MDSCs are independent risk factors in GBM. Steroidogenesis is central to tumor infiltration by immunosuppressive cells. Estrogenicity creates a niche filled by MDSCs/TAMs. Androgenicity is correlated with expression of male-specific antigens and RORC-Treg infiltration and activation. These processes can potentially be halted with steroid inhibitors, improving patient outcome. Sperm/testicular-specific protein shedding by GBM can be assessed by examining levels of anti-sperm/testicular antibodies in the patient serum. These discoveries unlock novel methods for detection and aiding the treatment of GBM. The data herein strongly support the view that the main Treg subtype supporting GBM ferocity is the RORC-Treg class, a class of Tregs normally associated with mucin-rich cancers such as colorectal and pancreatic.

**Supplementary Materials:** The following are available online at <https://www.mdpi.com/article/10.3390/ijms222010983/s1>.

**Author Contributions:** Conceptualization, M.A.S.; methodology, M.A.S.; investigation, M.A.S., A.M.B. and A.V.J.; formal analysis, M.A.S., A.M.B. and A.V.J.; data curation, M.A.S., A.M.B. and A.V.J.; writing—original draft preparation, M.A.S., A.M.B. and A.V.J.; writing—review and editing, M.A.S., A.M.B., A.V.J. and D.S.B.; project administration, D.S.B.; funding acquisition, D.S.B. All authors have read and agreed to the published version of the manuscript.

**Funding:** This work was supported by the Donna and Kenneth R. Peak Foundation, The Kenneth R. Peak Brain and Pituitary Center at Houston Methodist Hospital, The Taub Foundation, The Blanche Green Estate Fund of the Pauline Sterne Wolff Memorial Foundation, The John S. Dunn Foundation, Kelly Kicking Cancer, The Marilee A. and Gary M. Schwarz Foundation, The Houston Methodist Hospital Foundation, and the Verelan Foundation.

**Institutional Review Board Statement:** The study was conducted according to the guidelines of the Declaration of Helsinki and approved by the Institutional Review Board (or Ethics Committee) of Houston Methodist Hospital (IRB# Pro00014547 and approval 09/2016).

**Informed Consent Statement:** Informed consent was obtained from all subjects involved in the study.

**Data Availability Statement:** All transcriptome data used in the figures and in the Supplementary Data was obtained from the Firehose Legacy U133, the Firehose Legacy Agilent microarray, the CGGA and the Gravendeel databases, and references to these data are to be found within the text. The classification of GBM sub-types refined by utilizing the Gliovis platform, as were the graphics in some of the Supplementary Figures. (<http://gliovis.bioinfo.cnio.es/>). Derived data is available on request from the corresponding author.

**Acknowledgments:** We are grateful to the many patients and families who have helped us with our research. Special thanks to Jeanne Manalo and Aaron Thorne for editorial input.

**Conflicts of Interest:** The authors declare no conflict of interest. The funders had no role in the design of the study; in the collection, analyses, or interpretation of data, in the writing of the manuscript, or in the decision to publish the results.

## Appendix A

Supplemental Text: Granting of sexual privilege.

Epitope-Specific Tregs by Gender in Health and Disease: Background Immunology: Epitopes are uniquely recognized by T-cell receptors (TCRs) and B-cell receptors (BCRs), which are generated in T- and B-cells via the recombination of somatic genes [143]. Vast numbers of different TCRs and BCRs expressed by T and B cells allow these immune cells to interrogate the whole body for presence of 'non-Self'. When these receptors bind to an epitope, they either behave in a pro- or anti-inflammatory manner, dependent on the context. Naive CD4<sup>+</sup> T cells can become anti-inflammatory regulatory T cells (Tregs) by following three steps known as signals 1, 2, and 3 [144]. Signal 1 involves presenting epitopes to the TCR on the major histocompatibility complex (MHC) class II molecule of an antigen presenting cell, typically a dendritic cell (DC) or B cell. Signal 2 must follow, for proper activation and proliferation, from costimulatory molecules on the antigen-presenting cell, for example, CD80/CD86 with CD28 expressed on the T-cell surface. Signal 3, the cytokine environment, determines classification as either pro- or anti-inflammatory. IL-10 and TGFβ drive activated CD4<sup>+</sup> T-cells into Tregs, whereas IL-6 and IL-23 drive pro-inflammatory class-switching.

Determining 'Self' and 'non-Self': Estimates of potential numbers of TCRs produced by the recombination process range from >10<sup>20</sup> to 10<sup>61</sup> [145,146]. CD4<sup>+</sup> T cells, generated in the bone marrow, travel to the thymus and mature, undergoing thymopoiesis. Here, medullary thymic epithelial cells (mTECs) screen candidate CD4<sup>+</sup> T-cells for 'Self' recognition. The mTECs synthesize most 'Self' proteins produced in the body, chop them into epitopic peptides and present these epitopes on MHCII to candidate CD4<sup>+</sup> T-cells as 'Self'. Candidate CD4<sup>+</sup> T-cells whose TCR recognizes a proffered 'Self' epitope are either subject to clonal deletion (apoptosis) or become a Treg (provided presence of IL-2/IL-15/NFκβ signaling). The interrogation of CD4<sup>+</sup> T-cells by the mTECs with 'Self' epitopes is the major means of suppression of autoimmune T-cell activity [147]. Negative selection failure gives rise to autoreactive CD4<sup>+</sup> T-cells and autoimmune diseases [65]. When a B cell binds an antigen on its BCR, the antigen is internalized, directed toward lysosomes, proteolyzed into peptidyl fragments, bound to MHCII, exposed to the extracellular environment, and presented to immune cells. The proffered MHCII bound epitopes can be interrogated by the TCRs of CD4<sup>+</sup> T-cells. If the TCR of a T cell binds to an epitope presented on MHCII, then signal one is activated. Mutualistic signaling results in proliferation of these epitope-specific BCR/TCR interactions between the B cell and CD4<sup>+</sup> T cell, and the two cell types drive the proliferation and pro-inflammatory activation of the other. Activated B cells drive activated CD4<sup>+</sup> T-cell class switching into pro-inflammatory T-helper cells and B-cell proliferation, and differentiation is driven by the interaction with CD4<sup>+</sup> T-helper cells. B cells that bind and present 'Self' epitopes can give rise to autoimmune diseases. B-cell lineages that recognize 'Self' can be terminated or undergo class-switching into anti-inflammatory, regulatory B cells (Bregs). This lineage-editing or class-switching generally occurs when B cells present epitopes that are recognized by the TCR of a Treg. Normally, when a Treg recognizes a presented epitope via its TCR, it responds by sending a variety of death signals toward the B cell, causing apoptosis and the termination of the B-cell lineage [148]. However, sometimes the signaling directs the B cells to undergo a class-switch, and the B cell is directed to become an anti-inflammatory Breg.

Sexual privilege in males: Prepubescent boys have B cells whose BCRs recognize 'non-Self' sperm/testicular-specific epitopes. This results in circulating anti-sperm antibodies with CD4<sup>+</sup> T-cells that can bind sperm/testicular-specific epitopes [124]. At puberty, immune responses to 'non-Self' sperm/testicular-specific epitopes must be arrested. This is partially achieved by compartmentalization, with a blood–testis barrier created by tight-junctions between Sertoli cells. Additionally, Sertoli cells present male-specific epitopes on their MHCII [149], and drive TCR-activated CD4<sup>+</sup> T-cell class-switching into immunosuppressive Tregs. These Tregs maintain the anti-inflammatory environment of the testicle and edit the B-cell lineages which give rise to anti-sperm antibodies. This is achieved either

by lineage deletion or by class-switching into Bregs, resulting in anti-sperm antibodies disappearing after puberty [124]. The immunological 'self' is established long before puberty. At puberty, the maturation of testicles and the onset of sperm production presents boy's immune systems with a myriad of testicular and sperm specific autoantigens. If testicles are not afforded 'immune privilege', the immune system attacks the tissue, giving rise to autoimmune orchitis. This can occur spontaneously in patients with AIRE gene mutations, due to dysfunctional Tregs [150]. Tregs control tolerogenic versus autoimmune responses, with respect to sperm/testicular-specific antigens, as was demonstrated by Wheeler [122,151]. Vasectomy is a well-established form of birth control that does not lead to autoimmune orchitis, due to the presence of tolerogenic Tregs that are responsive to sperm/testicular-specific antigens [122,151,152]. Following vasectomy, the maintenance of tolerance toward sperm/testicular antigens leaking from the severed vas deferens requires a rapid response by Tregs [122,151,152]. The Tregs arrest the elevation of auto-antibodies and pathogenic CD4<sup>+</sup> T cells. This Treg tolerance to sperm/testicular antigens can be overcome by vaccination with sperm/testicular antigens. When volunteers with androgen-sensitive prostate cancer were injected with human testicular homogenate prior to their scheduled orchidectomy, they quickly developed autoimmune orchitis [125]. Experimental autoimmune orchitis (EAO) in animal models are well explored and give insights into the role of Tregs in immunotolerance toward sperm/testicular-specific antigens. Immune system attacks on testicles are seen when male mice are vaccinated with testicular homogenate or with sperm/testicular-specific proteins such as Zonadhesin (ZAN). EAO is caused by the expansion of sperm/testicular-specific CD4<sup>+</sup> T cells, sensitized toward sperm/testicular-specific epitopes, as was demonstrated by Feng and co-workers in elegant transplantation studies [153]. BALB/c donor mice were vaccinated with epididymal spermatozoa, giving rise to EAO. When sperm-specific CD4<sup>+</sup> T cells were extracted from these animals and transferred into naïve recipient mice, these unvaccinated males then developed EAO. Vasectomy exposes sperm/testicular antigens to the general immune system, away from a site of immune privilege. This provokes a B-cell response which elevates the levels of anti-sperm/testicular-specific antibodies, but does not lead to autoimmune orchitis. In contrast, when men were vaccinated with testicular homogenate, the immune response to the large bolus of sperm/testicular antigens overwhelmed the normal Treg maintenance of testicular privilege, resulting in autoimmune orchitis.

Sexual privilege in females. Following sexual activity, a woman's reproductive tract hosts a variety of male-specific antigens present in semen. Mounting an immune response toward male-specific antigens, leading to anti-sperm antibody production, renders women infertile. The presence of sperm/testicular-specific antibodies in women is a leading cause of infertility, generally treatable with steroids [124,154,155]. Semen's effect on the cervix allows women to host 'non-Self' male-specific antigens without mounting a pro-inflammatory response, through bestowing privilege. Upon encounter with healthy semen, it provides an exploitable immunological-niche geared toward the generation of epitope-specific Tregs and Bregs. Seminal fluid has high levels of prostaglandins and transforming growth factor- $\beta$  (TGF $\beta$ <sub>1</sub>, TGF $\beta$ <sub>2</sub> and TGF $\beta$ <sub>3</sub>) [156,157], Figure A1A. The cervix can also produce immunotolerant dendritic cells (tDCs) and myeloid-derived suppressor cells (MDSCs) [158–161]. The high levels of prostaglandin E2 (PGE2) in semen have been demonstrated to cause cervical DCs to take up a tolerogenic role [162]. PGE2 signaling alters cytokine production during antigen presentation, driving the production of IL-10 and TGF $\beta$ , promoting T-cell class-switching. Elevated levels of PGE2/TGF $\beta$  elicit the release of chemokines CXCL3 and CXCL8, which signal recruitment of monocytes from the periphery. These recruited monocytes are then presented with PGE2/TGF $\beta$  and undergo class-switching, becoming tDCs [158], which further release PGE2/TGF $\beta$  and IL-10 [159]. In the semenized cervix, large amounts of IL-11 are produced by the ectocervical cells. The combination of IL-11, via GP130 activation, with PGE2/TGF $\beta$ , has been shown to drive monocytes to become MDSCs [163]. Moreover, tDCs and MDSCs interact with each other and the ectocervix to generate positive feedback cytokine signaling, with tDC and MDSC

generation of PGE2, TGF $\beta$  and IL-10, to further enhance epitope-specific Treg generation. Women's dendritic cell response to sperm/testicular antigens in the presence of PGE2 gives rise to tolerogenic Treg lineages, sensitized to sperm/testicular-specific epitopes [158,164]. PGE2/TGF $\beta$  in semen also cause the ectocervix's endothelial and fibroblast cells to release immunomodulators and growth factors [165]. The apoptosis of activated B cells is driven by Tregs partially through CTLA4 and partially due to death signals granzyme, adenosine and FasL. CTLA4 can pluck CD80 and CD86 ligands out of the plasma membrane of B-cells by trans-endocytosis [166], triggering B-cell apoptosis, depicted in Supplemental Review Figure 1B. This CTLA4 mechanism drives the conversion of DCs from pro-inflammatory CD80<sup>Hi</sup>/CD86<sup>Hi</sup> into tolerogenic DCs CD80<sub>Low</sub>/CD86<sub>Low</sub> cells [167].

These Tregs allow women to tolerate sperm/testicular-specific antigens which are presented to them during coitus. In addition to mediating women's tolerogenicity toward sperm/testicular-specific antigens, these Tregs also form the basis of maternal fetal tolerance [156,168]. Fetal maternal tolerance is essential for a successful pregnancy. Tregs play an essential role in pregnancy and a women's tolerance to her unborn baby, primed by seminal fluid, as described above. Natural killer [NK] cells, which are CD16-CD56<sup>bright</sup>, CD4<sup>+</sup> T cells, and CD8<sup>+</sup> T cells, are all found to recognize trophoblasts that start to invade the endometrial tissue and uterine spiral artery after implantation, inducing a tolerogenic environment allowing for fetal development [169].

As is the case in men, the privilege women afford to sperm/testicular-specific antigens is conditional and women who are vaccinated with sperm/testicular-specific antigens exhibit an anti-immune response. Some 90 years ago, Baskin et al. injected women intramuscularly with their husbands' semen to cause production of anti-sperm antibodies; he proposed that this technique could be a means to allow women to control their fertility [170]. Such vaccination strategies to control fertility are being pursued currently [171].

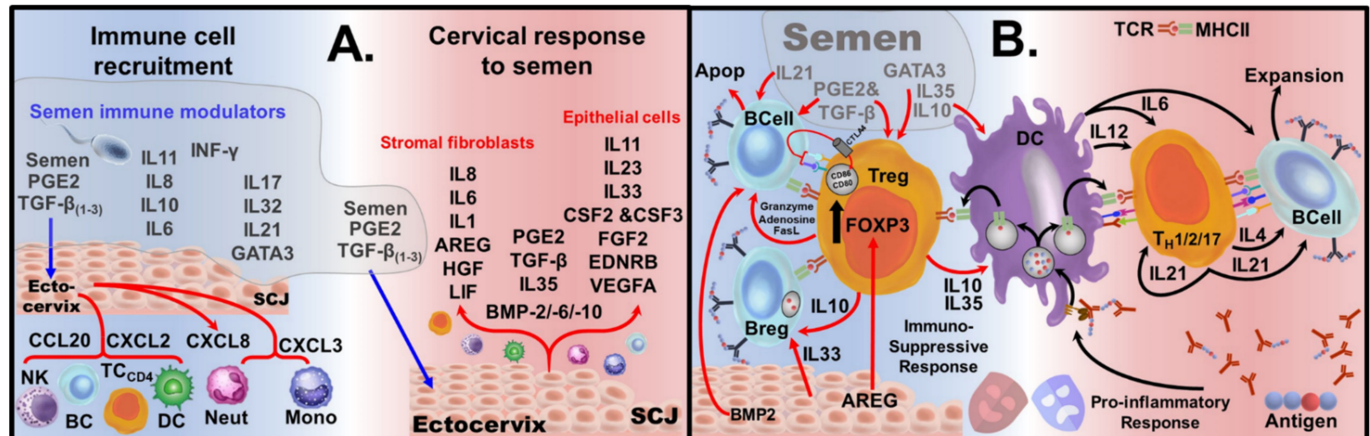


**Figure A1.** Cervical Response to Semen: (A) Major cytokines present in semen with the chemokine response of the cells of the ectocervix toward seminal PGE2/TGF $\beta$  cause the recruitment of immune cells (left). PGE2/TGF $\beta$  in semen cause ectocervix endothelial and fibroblast cells to release immunomodulators and growth factors (right). A combination of both male-derived and female-derived immunomodulators and growth factors are required for an optimal immune response by women toward the male-specific antigens present in semen. (B) (Left) Cytokines/growth factors generated by the interaction of semen with ectocervical cells drives the formation of Tregs, which are presented with recognized antigens. Instead of epitope presentation-induced activation of CD4<sup>+</sup> T cells and B cells, a seminized cervix has an array of cytokines/growth factors which generate epitope-specific Tregs. In addition, B cells which are activated by antigens bound to their BCRs can be driven to apoptosis, hence lineage deletion by death signals from Treg/cytokine/growth factors (IL21, PGE2, TNF $\beta$ , BMP2, granzyme, FasL and Adenosine). An alternative fate for antigen-activated B cells is class switching into Bregs, which can be induced by the presence of IL33 (cervical) and IL10. SCJ = squamous columnar junction; NK = Natural Killer Cells, TC = T cells, BC = B cells, DC = Dendritic Cells, Neut = Neutrophils, Mono = Monocytes AREG = Amphiregulin; Apop = apoptosis.

## References

1. Stupp, R.; Mason, W.P.; van den Bent, M.J.; Weller, M.; Fisher, B.; Taphoorn, M.J.; Belanger, K.; Brandes, A.A.; Marosi, C.; Bogdahn, U.; et al. Radiotherapy plus concomitant and adjuvant temozolomide for glioblastoma. *N. Engl. J. Med.* **2005**, *352*, 987–996. [[CrossRef](#)] [[PubMed](#)]
2. Marenco-Hillebrand, L.; Wijesekera, O.; Suarez-Meade, P.; Mampre, D.; Jackson, C.; Peterson, J.; Trifiletti, D.; Hammack, J.; Ortiz, K.; Lesser, E.; et al. Trends in glioblastoma: Outcomes over time and type of intervention: A systematic evidence based analysis. *J. Neurooncol.* **2020**, *147*, 297–307. [[CrossRef](#)] [[PubMed](#)]
3. Gilbert, M.R.; Dignam, J.J.; Armstrong, T.S.; Wefel, J.S.; Blumenthal, D.T.; Vogelbaum, M.A.; Colman, H.; Chakravarti, A.; Pugh, S.; Won, M.; et al. A randomized trial of bevacizumab for newly diagnosed glioblastoma. *N. Engl. J. Med.* **2014**, *370*, 699–708. [[CrossRef](#)] [[PubMed](#)]
4. Louis, D.N.; Perry, A.; Reifenberger, G.; von Deimling, A.; Figarella-Branger, D.; Cavenee, W.K.; Ohgaki, H.; Wiestler, O.D.; Kleihues, P.; Ellison, D.W. The 2016 World Health Organization Classification of Tumors of the Central Nervous System: A summary. *Acta Neuropathol.* **2016**, *131*, 803–820. [[CrossRef](#)] [[PubMed](#)]
5. Stringfield, O.; Arrington, J.A.; Johnston, S.K.; Rognin, N.G.; Peeri, N.C.; Balagurunathan, Y.; Jackson, P.R.; Clark-Swanson, K.R.; Swanson, K.R.; Egan, K.M.; et al. Multiparameter MRI Predictors of Long-Term Survival in Glioblastoma Multiforme. *Tomography* **2019**, *5*, 135–144. [[CrossRef](#)]
6. Villanueva-Meyer, J.E.; Mabray, M.C.; Cha, S. Current Clinical Brain Tumor Imaging. *Neurosurgery* **2017**, *81*, 397–415. [[CrossRef](#)] [[PubMed](#)]
7. Huang, S.; Michalek, J.E.; Reardon, D.A.; Wen, P.Y.; Floyd, J.R.; Fox, P.T.; Clarke, G.D.; Jerabek, P.A.; Schmainda, K.M.; Muzi, M.; et al. Assessment of tumor hypoxia and perfusion in recurrent glioblastoma following bevacizumab failure using MRI and 18F-FMISO PET. *Sci. Rep.* **2021**, *11*, 7632. [[CrossRef](#)] [[PubMed](#)]
8. Sharpe, M.A.; Ismail, N.; Baskin, D.S. Metabolic sculpting of the mitochondria, cell signaling and the cancer phenotype. *Transl. Cancer Res.* **2017**, *6*, S182–S188. [[CrossRef](#)]
9. Krzeslak, A.; Wojcik-Krowiranda, K.; Forma, E.; Jozwiak, P.; Romanowicz, H.; Bienkiewicz, A.; Brys, M. Expression of GLUT1 and GLUT3 glucose transporters in endometrial and breast cancers. *Pathol. Oncol. Res.* **2012**, *18*, 721–728. [[CrossRef](#)]
10. Flavahan, W.A.; Wu, Q.; Hitomi, M.; Rahim, N.; Kim, Y.; Sloan, A.E.; Weil, R.J.; Nakano, I.; Sarkaria, J.N.; Stringer, B.W.; et al. Brain Tumor Initiating Cells Adapt to Restricted Nutrition through Preferential Glucose Uptake. *Nat. Neurosci.* **2013**, *16*, 1373–1382. [[CrossRef](#)]
11. Masin, M.; Vazquez, J.; Rossi, S.; Groeneveld, S.; Samson, N.; Schwalie, P.C.; Deplancke, B.; Frawley, L.E.; Gouttenoire, J.; Moradpour, D.; et al. GLUT3 is induced during epithelial-mesenchymal transition and promotes tumor cell proliferation in non-small cell lung cancer. *Cancer Metab.* **2014**, *2*, 11. [[CrossRef](#)]
12. Luo, X.; Xu, S.; Zhong, Y.; Tu, T.; Xu, Y.; Li, X.; Wang, B.; Yang, F. High gene expression levels of VEGFA and CXCL8 in the peritumoral brain zone are associated with the recurrence of glioblastoma: A bioinformatics analysis. *Oncol. Lett.* **2019**, *18*, 6171–6179. [[CrossRef](#)]
13. Shen, G.M.; Zhao, Y.Z.; Chen, M.T.; Zhang, F.L.; Liu, X.L.; Wang, Y.; Liu, C.Z.; Yu, J.; Zhang, J.W. Hypoxia-inducible factor-1 (HIF-1) promotes LDL and VLDL uptake through inducing VLDLR under hypoxia. *Biochem. J.* **2012**, *441*, 675–683. [[CrossRef](#)] [[PubMed](#)]
14. Masoud, G.N.; Li, W. HIF-1 $\alpha$  pathway: Role, regulation and intervention for cancer therapy. *Acta Pharm. Sin. B* **2015**, *5*, 378–389. [[CrossRef](#)]
15. Krzywinska, E.; Stockmann, C. Hypoxia, Metabolism and Immune Cell Function. *Biomedicines* **2018**, *6*, 56. [[CrossRef](#)] [[PubMed](#)]
16. Mi, Y.; Guo, N.; Luan, J.; Cheng, J.; Hu, Z.; Jiang, P.; Jin, W.; Gao, X. The Emerging Role of Myeloid-Derived Suppressor Cells in the Glioma Immune Suppressive Microenvironment. *Front. Immunol.* **2020**, *11*, 737. [[CrossRef](#)] [[PubMed](#)]
17. Bayik, D.; Zhou, Y.; Park, C.; Hong, C.; Vail, D.; Silver, D.J.; Lauko, A.; Roversi, G.; Watson, D.C.; Lo, A.; et al. Myeloid-Derived Suppressor Cell Subsets Drive Glioblastoma Growth in a Sex-Specific Manner. *Cancer Discov.* **2020**, *10*, 1210–1225. [[CrossRef](#)]
18. Landry, A.P.; Balas, M.; Alli, S.; Spears, J.; Zador, Z. Distinct regional ontogeny and activation of tumor associated macrophages in human glioblastoma. *Sci. Rep.* **2020**, *10*, 19542. [[CrossRef](#)]
19. Takenaka, M.C.; Gabriely, G.; Rothhammer, V.; Mascanfroni, I.D.; Wheeler, M.A.; Chao, C.-C.; Gutiérrez-Vázquez, C.; Kenison, J.; Tjon, E.C.; Barroso, A.; et al. Control of tumor-associated macrophages and T cells in glioblastoma via AHR and CD39. *Nat. Neurosci.* **2019**, *22*, 729–740. [[CrossRef](#)]
20. Miska, J.; Rashidi, A.; Chang, A.L.; Muroski, M.E.; Han, Y.; Zhang, L.; Lesniak, M.S. Anti-GITR therapy promotes immunity against malignant glioma in a murine model. *Cancer Immunol. Immunother.* **2016**, *65*, 1555–1567. [[CrossRef](#)]
21. Sayour, E.J.; McLendon, P.; McLendon, R.; De Leon, G.; Reynolds, R.; Kresak, J.; Sampson, J.H.; Mitchell, D.A. Increased proportion of FoxP3+ regulatory T cells in tumor infiltrating lymphocytes is associated with tumor recurrence and reduced survival in patients with glioblastoma. *Cancer Immunol. Immunother.* **2015**, *64*, 419–427. [[CrossRef](#)] [[PubMed](#)]
22. Sieow, J.L.; Gun, S.Y.; Wong, S.C. The Sweet Surrender: How Myeloid Cell Metabolic Plasticity Shapes the Tumor Microenvironment. *Front. Cell Dev. Biol.* **2018**, *6*, 168. [[CrossRef](#)] [[PubMed](#)]
23. Guo, X.Y.; Zhang, G.H.; Wang, Z.N.; Duan, H.; Xie, T.; Liang, L.; Cui, R.; Hu, H.R.; Wu, Y.; Dong, J.J.; et al. A novel Foxp3-related immune prognostic signature for glioblastoma multiforme based on immunogenomic profiling. *Aging* **2021**, *13*, 3501–3517. [[CrossRef](#)] [[PubMed](#)]

24. Liu, F.; Huang, J.; Liu, X.; Cheng, Q.; Luo, C.; Liu, Z. CTLA-4 correlates with immune and clinical characteristics of glioma. *Cancer Cell Int.* **2020**, *20*, 7. [[CrossRef](#)]
25. Aslan, K.; Turco, V.; Blobner, J.; Sonner, J.K.; Liuzzi, A.R.; Núñez, N.G.; De Feo, D.; Kickingreder, P.; Fischer, M.; Green, E.; et al. Heterogeneity of response to immune checkpoint blockade in hypermutated experimental gliomas. *Nat. Commun.* **2020**, *11*, 931. [[CrossRef](#)]
26. Patel, M.A.; Kim, J.E.; Theodoros, D.; Tam, A.; Velarde, E.; Kochel, C.M.; Francica, B.; Nirschl, T.R.; Ghasemzadeh, A.; Mathios, D.; et al. Agonist anti-GITR monoclonal antibody and stereotactic radiation induce immune-mediated survival advantage in murine intracranial glioma. *J. Immunother. Cancer* **2016**, *4*, 28. [[CrossRef](#)]
27. Takashima, Y.; Kawaguchi, A.; Hayano, A.; Yamanaka, R. CD276 and the gene signature composed of GATA3 and LGALS3 enable prognosis prediction of glioblastoma multiforme. *PLoS ONE* **2019**, *14*, e0216825. [[CrossRef](#)]
28. Ayyoub, M.; Deknuydt, F.; Raimbaud, I.; Dousset, C.; Leveque, L.; Bioley, G.; Valmori, D. Human memory FOXP3+ Tregs secrete IL-17 ex vivo and constitutively express the T(H)17 lineage-specific transcription factor RORgamma t. *Proc. Natl. Acad. Sci. USA* **2009**, *106*, 8635–8640. [[CrossRef](#)]
29. Yang, B.H.; Hagemann, S.; Mamareli, P.; Lauer, U.; Hoffmann, U.; Beckstette, M.; Föhse, L.; Prinz, I.; Pezoldt, J.; Suerbaum, S.; et al. Foxp3+ T cells expressing RORγt represent a stable regulatory T-cell effector lineage with enhanced suppressive capacity during intestinal inflammation. *Mucosal Immunol.* **2016**, *9*, 444–457. [[CrossRef](#)]
30. Weaver, C.T.; Hatton, R.D. Interplay between the TH17 and TReg cell lineages: A (co-)evolutionary perspective. *Nat. Rev. Immunol.* **2009**, *9*, 883–889. [[CrossRef](#)]
31. Herrnstadt, G.R.; Steinmetz, O.M. The role of Treg subtypes in glomerulonephritis. *Cell Tissue Res.* **2020**. [[CrossRef](#)]
32. Kluger, M.A.; Meyer, M.C.; Nosko, A.; Goerke, B.; Luig, M.; Wegscheid, C.; Tiegs, G.; Stahl, R.A.; Panzer, U.; Steinmetz, O.M. RORγt(+)Foxp3(+) Cells are an Independent Bifunctional Regulatory T Cell Lineage and Mediate Crescentic GN. *J. Am. Soc. Nephrol.* **2016**, *27*, 454–465. [[CrossRef](#)]
33. Le Tortorec, A.; Matusali, G.; Mahé, D.; Aubry, F.; Mazaud-Guittot, S.; Houzet, L.; Dejuq-Rainsford, N. From Ancient to Emerging Infections: The Odyssey of Viruses in the Male Genital Tract. *Physiol. Rev.* **2020**, *100*, 1349–1414. [[CrossRef](#)]
34. Teles, A.; Schumacher, A.; Kühnle, M.; Linzke, N.; Thuere, C.; Reichardt, P.; Tadokoro, C.; Hämmerling, G.; Zenclussen, A. Control of Uterine Microenvironment by Foxp3+ Cells Facilitates Embryo Implantation. *Front. Immunol.* **2013**, *4*, 158. [[CrossRef](#)] [[PubMed](#)]
35. He, S.M.; Xing, F.Q.; Sui, H.; Wang, Y.L.; Mai, X.F.; Luo, Z.Q.; Chen, X.Q.; Chen, G.H.; Kong, Z.J. [CA 125 expression in cervical and vaginal secretions in women in normal reproductive period]. *Nan Fang Yi Ke Da Xue Xue Bao* **2010**, *30*, 173–175. [[PubMed](#)]
36. Tavmergen, E.; Sendag, F.; Goker, E.N.T.; Levi, R. Value of serum CA-125 concentrations as predictors of pregnancy in assisted reproduction cycles. *Hum. Reprod.* **2001**, *16*, 1129–1134. [[CrossRef](#)] [[PubMed](#)]
37. Geva, E.; Arava, J.; Lerner-Geva, L.; Hareuveni, M.; Lessing, J.B.; Ballas, S.; Amit, A. The ratio between carcinoma antigen-125 levels in the seminal plasma and serum may be a marker for fertilization in intracytoplasmic sperm injection. *Fertil. Steril.* **1997**, *68*, 1120–1124. [[CrossRef](#)]
38. Reinartz, S.R.; Pfisterer, J.; du Bois, A.; Jackisch, C.; Baumann, K.H.; Wagner, U. Suppressiveness activity rather than frequency of FoxP3(+) regulatory T cells is essential for CA-125-specific T-cell activation after abagovomab treatment. *Hum. Immunol.* **2010**, *71*, 36–44. [[CrossRef](#)]
39. Pinget, G.V.; Corpuz, T.M.; Stolp, J.; Lousberg, E.L.; Diener, K.R.; Robertson, S.A.; Sprent, J.; Webster, K.E. The majority of murine γδ T cells at the maternal–fetal interface in pregnancy produce IL-17. *Immunol. Cell Biol.* **2016**, *94*, 623–630. [[CrossRef](#)] [[PubMed](#)]
40. Gallino, L.; Hauk, V.; Fernández, L.; Soczewski, E.; Gori, S.; Grasso, E.; Calo, G.; Saraco, N.; Berensztejn, E.; Waschek, J.A.; et al. VIP Promotes Recruitment of Tregs to the Uterine–Placental Interface During the Peri-Implantation Period to Sustain a Tolerogenic Microenvironment. *Front. Immunol.* **2020**, *10*, 2907. [[CrossRef](#)]
41. Robertson, S.A.; Care, A.S.; Moldenhauer, L.M. Regulatory T cells in embryo implantation and the immune response to pregnancy. *J. Clin. Investig.* **2018**, *128*, 4224–4235. [[CrossRef](#)]
42. Wilharm, A.; Brigas, H.C.; Sandrock, I.; Ribeiro, M.; Amado, T.; Reinhardt, A.; Demera, A.; Hoenicke, L.; Strowig, T.; Carvalho, T.; et al. Microbiota-dependent expansion of testicular IL-17-producing Vγ6+ γδ T cells upon puberty promotes local tissue immune surveillance. *Mucosal Immunol.* **2021**, *14*, 242–252. [[CrossRef](#)] [[PubMed](#)]
43. Franke, F.; Kraus, S.; Pauls, K.; Lalani, E.-N.; Bergmann, M. MUC1 in normal and impaired spermatogenesis. *Mol. Hum. Reprod.* **2001**, *7*, 505–512. [[CrossRef](#)] [[PubMed](#)]
44. Russo, C.L.; Spurr-Michaud, S.; Tisdale, A.; Pudney, J.; Anderson, D.; Gipson, I.K. Mucin gene expression in human male urogenital tract epithelia. *Hum. Reprod.* **2006**, *21*, 2783–2793. [[CrossRef](#)] [[PubMed](#)]
45. Shin, B.; Benavides, G.A.; Geng, J.; Koralov, S.B.; Hu, H.; Darley-Usmar, V.M.; Harrington, L.E. Mitochondrial Oxidative Phosphorylation Regulates the Fate Decision between Pathogenic Th17 and Regulatory T Cells. *Cell Rep.* **2020**, *30*, 1898–1909.e4. [[CrossRef](#)] [[PubMed](#)]
46. Zheng, L.; Kelly, C.J.; Colgan, S.P. Physiologic hypoxia and oxygen homeostasis in the healthy intestine. A Review in the Theme: Cellular Responses to Hypoxia. *Am. J. Physiol. Cell Physiol.* **2015**, *309*, C350–C360. [[CrossRef](#)] [[PubMed](#)]
47. Bohlen, H.G. Intestinal mucosal oxygenation influences absorptive hyperemia. *Am. J. Physiol.* **1980**, *239*, H489–H493. [[CrossRef](#)]

48. Dominguez, J.M.; Davis, R.T.; McCullough, D.J.; Stabley, J.N.; Behnke, B.J. Aging and exercise training reduce testes microvascular PO<sub>2</sub> and alter vasoconstrictor responsiveness in testicular arterioles. *Am. J. Physiol. Regul. Integr. Comp. Physiol.* **2011**, *301*, R801–R810. [[CrossRef](#)]
49. Movsas, B.; Chapman, J.D.; Hanlon, A.L.; Horwitz, E.M.; Greenberg, R.E.; Stobbe, C.; Hanks, G.E.; Pollack, A. Hypoxic prostate/muscle po<sub>2</sub> ratio predicts for biochemical failure in patients with prostate cancer: Preliminary findings. *Urology* **2002**, *60*, 634–639. [[CrossRef](#)]
50. Fukuda, M.; Fukuda, K.; Ranoux, C. Unexpected low oxygen tension of intravaginal culture. *Hum. Reprod.* **1996**, *11*, 1293–1295. [[CrossRef](#)]
51. Rashad, A.L.; Toffler, W.L.; Wolf, N.; Thornburg, K.; Kirk, E.P.; Ellis, G.; Whitehead, W.E. Vaginal PO<sub>2</sub> in healthy women and in women infected with *Trichomonas vaginalis*: Potential implications for metronidazole therapy. *Am. J. Obs. Gynecol.* **1992**, *166*, 620–624. [[CrossRef](#)]
52. Hill, D.R.; Brunner, M.E.; Schmitz, D.C.; Davis, C.C.; Flood, J.A.; Schlievert, P.M.; Wang-Weigand, S.Z.; Osborn, T.W. In vivo assessment of human vaginal oxygen and carbon dioxide levels during and post menses. *J. Appl. Physiol.* **2005**, *99*, 1582–1591. [[CrossRef](#)] [[PubMed](#)]
53. McKeown, S.R. Defining normoxia, physoxia and hypoxia in tumours-implications for treatment response. *Br. J. Radiol.* **2014**, *87*, 20130676. [[CrossRef](#)] [[PubMed](#)]
54. Vaupel, P.; Höckel, M.; Mayer, A. Detection and characterization of tumor hypoxia using pO<sub>2</sub> histography. *Antioxid. Redox Signal.* **2007**, *9*, 1221–1235. [[CrossRef](#)] [[PubMed](#)]
55. Pinacho-Garcia, L.M.; Valdez, R.A.; Navarrete, A.; Cabeza, M.; Segovia, J.; Romano, M.C. The effect of finasteride and dutasteride on the synthesis of neurosteroids by glioblastoma cells. *Steroids* **2020**, *155*, 108556. [[CrossRef](#)] [[PubMed](#)]
56. Orozco, M.; Valdez, R.A.; Ramos, L.; Cabeza, M.; Segovia, J.; Romano, M.C. Dutasteride combined with androgen receptor antagonists inhibit glioblastoma U87 cell metabolism, proliferation, and invasion capacity: Androgen regulation. *Steroids* **2020**, *164*, 108733. [[CrossRef](#)]
57. Chuang, J.Y.; Lo, W.L.; Ko, C.Y.; Chou, S.Y.; Chen, R.M.; Chang, K.Y.; Hung, J.J.; Su, W.C.; Chang, W.C.; Hsu, T.I. Upregulation of CYP17A1 by Sp1-mediated DNA demethylation confers temozolomide resistance through DHEA-mediated protection in glioma. *Oncogenesis* **2017**, *6*, e339. [[CrossRef](#)]
58. Lin, H.Y.; Ko, C.Y.; Kao, T.J.; Yang, W.B.; Tsai, Y.T.; Chuang, J.Y.; Hu, S.L.; Yang, P.Y.; Lo, W.L.; Hsu, T.I. CYP17A1 Maintains the Survival of Glioblastomas by Regulating SARI-Mediated Endoplasmic Reticulum Health and Redox Homeostasis. *Cancers* **2019**, *11*, 1378. [[CrossRef](#)] [[PubMed](#)]
59. Rižner, T.L.; Penning, T.M. Role of aldo-keto reductase family 1 (AKR1) enzymes in human steroid metabolism. *Steroids* **2014**, *79*, 49–63. [[CrossRef](#)]
60. Hernández-Vega, A.M.; Del Moral-Morales, A.; Zamora-Sánchez, C.J.; Piña-Medina, A.G.; González-Arenas, A.; Camacho-Arroyo, I. Estradiol Induces Epithelial to Mesenchymal Transition of Human Glioblastoma Cells. *Cells* **2020**, *9*, 1930. [[CrossRef](#)]
61. Zhao, N.; Wang, F.; Ahmed, S.; Liu, K.; Zhang, C.; Cathcart, S.J.; DiMaio, D.J.; Punsoni, M.; Guan, B.; Zhou, P.; et al. Androgen Receptor, Although Not a Specific Marker For, Is a Novel Target to Suppress Glioma Stem Cells as a Therapeutic Strategy for Glioblastoma. *Front. Oncol.* **2021**, *11*, 1696.
62. Adurthi, S.; Kumar, M.M.; Vinodkumar, H.S.; Mukherjee, G.; Krishnamurthy, H.; Acharya, K.K.; Bafna, U.D.; Uma, D.K.; Abhishekh, B.; Krishna, S.; et al. Oestrogen Receptor- $\alpha$  binds the FOXP3 promoter and modulates regulatory T-cell function in human cervical cancer. *Sci. Rep.* **2017**, *7*, 17289. [[CrossRef](#)] [[PubMed](#)]
63. Ishikawa, A.; Wada, T.; Nishimura, S.; Ito, T.; Okekawa, A.; Onogi, Y.; Watanabe, E.; Sameshima, A.; Tanaka, T.; Tsuneki, H.; et al. Estrogen regulates sex-specific localization of regulatory T cells in adipose tissue of obese female mice. *PLoS ONE* **2020**, *15*, e0230885. [[CrossRef](#)] [[PubMed](#)]
64. Mjösberg, J.; Svensson, J.; Johansson, E.; Hellström, L.; Casas, R.; Jenmalm, M.C.; Boij, R.; Matthiesen, L.; Jönsson, J.L.; Berg, G.; et al. Systemic reduction of functionally suppressive CD4<sup>dim</sup>CD25<sup>high</sup>Foxp3<sup>+</sup> Tregs in human second trimester pregnancy is induced by progesterone and 17 $\beta$ -estradiol. *J. Immunol.* **2009**, *183*, 759–769. [[CrossRef](#)]
65. Zhu, M.L.; Bakhru, P.; Conley, B.; Nelson, J.S.; Free, M.; Martin, A.; Starmer, J.; Wilson, E.M.; Su, M.A. Sex bias in CNS autoimmune disease mediated by androgen control of autoimmune regulator. *Nat. Commun.* **2016**, *7*, 11350. [[CrossRef](#)] [[PubMed](#)]
66. Walecki, M.; Eisel, F.; Klug, J.; Baal, N.; Paradowska-Dogan, A.; Wahle, E.; Hackstein, H.; Meinhardt, A.; Fijak, M. Androgen receptor modulates Foxp3 expression in CD4<sup>+</sup>CD25<sup>+</sup>Foxp3<sup>+</sup> regulatory T-cells. *Mol. Biol. Cell* **2015**, *26*, 2845–2857. [[CrossRef](#)]
67. Consiglio, C.R.; Udartseva, O.; Ramsey, K.D.; Bush, C.; Gollnick, S.O. Enzalutamide, an Androgen Receptor Antagonist, Enhances Myeloid Cell-Mediated Immune Suppression and Tumor Progression. *Cancer Immunol. Res.* **2020**, *8*, 1215–1227. [[CrossRef](#)]
68. Sharpe, M.A.; Ijare, O.B.; Baskin, D.S.; Baskin, A.M.; Baskin, B.N.; Pichumani, K. The Leloir Cycle in Glioblastoma: Galactose Scavenging and Metabolic Remodeling. *Cancers* **2021**, *13*, 1815. [[CrossRef](#)]
69. Shraibman, B.; Barnea, E.; Kadosh, D.M.; Haimovich, Y.; Slobodin, G.; Rosner, I.; López-Larrea, C.; Hilf, N.; Kuttruff, S.; Song, C.; et al. Identification of Tumor Antigens Among the HLA Peptidomes of Glioblastoma Tumors and Plasma. *Mol. Cell. Proteom.* **2018**, *17*, 2132–2145. [[CrossRef](#)]
70. Akiyama, Y.; Komiyama, M.; Miyata, H.; Yagoto, M.; Ashizawa, T.; Iizuka, A.; Oshita, C.; Kume, A.; Nogami, M.; Ito, I.; et al. Novel cancer-testis antigen expression on glioma cell lines derived from high-grade glioma patients. *Oncol. Rep.* **2014**, *31*, 1683–1690. [[CrossRef](#)]

71. Freitas, M.; Malheiros, S.; Stávale, J.N.; Biassi, T.P.; Zamunér, F.T.; de Souza Begnami, M.; Soares, F.A.; Vettore, A.L. Expression of cancer/testis antigens is correlated with improved survival in glioblastoma. *Oncotarget* **2013**, *4*, 636–646. [[CrossRef](#)] [[PubMed](#)]
72. Sreekanthreddy, P.; Srinivasan, H.; Kumar, D.M.; Nijaguna, M.B.; Sridevi, S.; Vrinda, M.; Arivazhagan, A.; Balasubramaniam, A.; Hegde, A.S.; Chandramouli, B.A.; et al. Identification of potential serum biomarkers of glioblastoma: Serum osteopontin levels correlate with poor prognosis. *Cancer Epidemiol. Biomark. Prev.* **2010**, *19*, 1409–1422. [[CrossRef](#)]
73. Jones, K.; Ballesteros, A.; Mentink-Kane, M.; Warren, J.; Rattila, S.; Malech, H.; Kang, E.; Dveksler, G. PSG9 Stimulates Increase in FoxP3+ Regulatory T-Cells through the TGF- $\beta$ 1 Pathway. *PLoS ONE* **2016**, *11*, e0158050. [[CrossRef](#)] [[PubMed](#)]
74. Timganova, V.P.; Zamorina, S.A.; Litvinova, L.S.; Todosenko, N.M.; Bochkova, M.S.; Khramtsov, P.V.; Rayev, M.B. The effects of human pregnancy-specific  $\beta$ 1-glycoprotein preparation on Th17 polarization of CD4+ cells and their cytokine profile. *BMC Immunol.* **2020**, *21*, 56. [[CrossRef](#)]
75. Zheng, B. Expression and clinical importance of a newly discovered alternative splice variant of the gene for acrosin binding protein found in human brain tumors. *Asian Biomed.* **2020**, *14*, 243–252. [[CrossRef](#)]
76. Li, X.; Yan, J.; Fan, R.; Luo, B.; Zhang, Q.; Lin, Y.; Zhou, S.; Luo, G.; Xie, X.; Xiao, S. Serum immunoreactivity of cancer/testis antigen OY-TES-1 and its tissues expression in glioma. *Oncol. Lett.* **2017**, *13*, 3080–3086. [[CrossRef](#)]
77. Redzovic, A.; Laskarin, G.; Dominovic, M.; Haller, H.; Rukavina, D. Mucins Help to Avoid Alloreactivity at the Maternal Fetal Interface. *Clin. Dev. Immunol.* **2013**, *2013*, 542152. [[CrossRef](#)] [[PubMed](#)]
78. Wei, X.; Xu, H.; Kufe, D. MUC1 Oncoprotein Stabilizes and Activates Estrogen Receptor  $\alpha$ . *Mol. Cell* **2006**, *21*, 295–305. [[CrossRef](#)]
79. Meseguer, M.; Aplin, J.D.; Caballero-Campo, P.; O'Connor, J.E.; Martín, J.C.; Remohí, J.; Pellicer, A.; Simón, C. Human Endometrial Mucin MUC1 Is Up-Regulated by Progesterone and Down-Regulated In Vitro by the Human Blastocyst1. *Biol. Reprod.* **2001**, *64*, 590–601. [[CrossRef](#)]
80. Aubert, S.; Fauquette, V.; Hémon, B.; Lepoivre, R.; Briez, N.; Bernard, D.; Van Seuning, I.; Leroy, X.; Perrais, M. MUC1, a New Hypoxia Inducible Factor Target Gene, Is an Actor in Clear Renal Cell Carcinoma Tumor Progression. *Cancer Res.* **2009**, *69*, 5707. [[CrossRef](#)]
81. Pyzer, A.R.; Stroopinsky, D.; Rajabi, H.; Washington, A.; Tagde, A.; Coll, M.; Fung, J.; Bryant, M.P.; Cole, L.; Palmer, K.; et al. MUC1-mediated induction of myeloid-derived suppressor cells in patients with acute myeloid leukemia. *Blood* **2017**, *129*, 1791–1801. [[CrossRef](#)] [[PubMed](#)]
82. Kim, S.; Seo, Y.; Chowdhury, T.; Yu, H.J.; Lee, C.E.; Kim, K.-M.; Kang, H.; Kim, H.J.; Park, S.-J.; Kim, K.; et al. Inhibition of MUC1 exerts cell-cycle arrest and telomerase suppression in glioblastoma cells. *Sci. Rep.* **2020**, *10*, 18238. [[CrossRef](#)]
83. Phillips, H.S.; Kharbanda, S.; Chen, R.; Forrest, W.F.; Soriano, R.H.; Wu, T.D.; Misra, A.; Nigro, J.M.; Colman, H.; Soroceanu, L.; et al. Molecular subclasses of high-grade glioma predict prognosis, delineate a pattern of disease progression, and resemble stages in neurogenesis. *Cancer Cell* **2006**, *9*, 157–173. [[CrossRef](#)]
84. Verhaak, R.G.; Hoadley, K.A.; Purdom, E.; Wang, V.; Qi, Y.; Wilkerson, M.D.; Miller, C.R.; Ding, L.; Golub, T.; Mesirov, J.P.; et al. Integrated genomic analysis identifies clinically relevant subtypes of glioblastoma characterized by abnormalities in PDGFRA, IDH1, EGFR, and NF1. *Cancer Cell* **2010**, *17*, 98–110. [[CrossRef](#)] [[PubMed](#)]
85. Teo, W.-Y.; Sekar, K.; Seshachalam, P.; Shen, J.; Chow, W.-Y.; Lau, C.C.; Yang, H.; Park, J.; Kang, S.-G.; Li, X.; et al. Relevance of a TCGA-derived Glioblastoma Subtype Gene-Classifer among Patient Populations. *Sci. Rep.* **2019**, *9*, 7442. [[CrossRef](#)]
86. Bowman, R.L.; Wang, Q.; Carro, A.; Verhaak, R.G.W.; Squatrito, M. GlioVis data portal for visualization and analysis of brain tumor expression datasets. *Neuro Oncol.* **2017**, *19*, 139–141. [[CrossRef](#)] [[PubMed](#)]
87. Ohue, Y.; Nishikawa, H. Regulatory T (Treg) cells in cancer: Can Treg cells be a new therapeutic target? *Cancer Sci.* **2019**, *110*, 2080–2089. [[CrossRef](#)] [[PubMed](#)]
88. Knee, D.A.; Hewes, B.; Brogdon, J.L. Rationale for anti-GITR cancer immunotherapy. *Eur. J. Cancer* **2016**, *67*, 1–10. [[CrossRef](#)]
89. Kim, B.-S.; Lu, H.; Ichiyama, K.; Chen, X.; Zhang, Y.-B.; Mistry, N.A.; Tanaka, K.; Lee, Y.-H.; Nuriyeva, R.; Zhang, L.; et al. Generation of ROR $\gamma$ t(+) Antigen-Specific T Regulatory 17 Cells from Foxp3(+) Precursors in Autoimmunity. *Cell Rep.* **2017**, *21*, 195–207. [[CrossRef](#)]
90. Wohlfert, E.A.; Grainger, J.R.; Bouladoux, N.; Konkel, J.E.; Oldenhove, G.; Ribeiro, C.H.; Hall, J.A.; Yagi, R.; Naik, S.; Bhairavahotla, R.; et al. GATA3 controls Foxp3+ regulatory T cell fate during inflammation in mice. *J. Clin. Investig.* **2011**, *121*, 4503–4515. [[CrossRef](#)]
91. Ho, I.C.; Tai, T.-S.; Pai, S.-Y. GATA3 and the T-cell lineage: Essential functions before and after T-helper-2-cell differentiation. *Nat. Rev. Immunol.* **2009**, *9*, 125–135. [[CrossRef](#)]
92. Sousa, C.; Golebiewska, A.; Poovathingal, S.K.; Kaoma, T.; Pires-Afonso, Y.; Martina, S.; Coowar, D.; Azuaje, F.; Skupin, A.; Balling, R.; et al. Single-cell transcriptomics reveals distinct inflammation-induced microglia signatures. *EMBO Rep.* **2018**, *19*, e46171. [[CrossRef](#)]
93. Kuo, L.-C.; Cheng, L.-C.; Lee, C.-H.; Lin, C.-J.; Chen, P.-Y.; Li, L.-A. Estrogen and cigarette sidestream smoke particulate matter exhibit ER $\alpha$ -dependent tumor-promoting effects in lung adenocarcinoma cells. *Am. J. Physiol. Lung Cell. Mol. Physiol.* **2017**, *313*, L477–L490. [[CrossRef](#)]
94. Dassen, H.; Punyadeera, C.; Kamps, R.; Klomp, J.; Dunselman, G.; Dijcks, F.; de Goeij, A.; Ederveen, A.; Groothuis, P. Progesterone regulation of implantation-related genes: New insights into the role of oestrogen. *Cell. Mol. Life Sci.* **2007**, *64*, 1009–1032. [[CrossRef](#)] [[PubMed](#)]

95. Droog, M.; Nevedomskaya, E.; Kim, Y.; Severson, T.; Flach, K.D.; Opdam, M.; Schuurman, K.; Gradowska, P.; Hauptmann, M.; Dackus, G.; et al. Comparative Cistromics Reveals Genomic Cross-talk between FOXA1 and ER $\alpha$  in Tamoxifen-Associated Endometrial Carcinomas. *Cancer Res.* **2016**, *76*, 3773–3784. [[CrossRef](#)] [[PubMed](#)]
96. Chan, H.J.; Li, H.; Liu, Z.; Yuan, Y.C.; Mortimer, J.; Chen, S. SERPINA1 is a direct estrogen receptor target gene and a predictor of survival in breast cancer patients. *Oncotarget* **2015**, *6*, 25815–25827. [[CrossRef](#)] [[PubMed](#)]
97. Li, Q.; He, H.; Zhang, Y.-L.; Li, X.-M.; Guo, X.; Huo, R.; Bi, Y.; Li, J.; Fan, H.-Y.; Sha, J. Phosphoinositide 3-kinase p110 $\delta$  mediates estrogen- and FSH-stimulated ovarian follicle growth. *Mol. Endocrinol.* **2013**, *27*, 1468–1482. [[CrossRef](#)] [[PubMed](#)]
98. Du, M.J.; Chen, X.D.; Zhou, X.L.; Wan, Y.J.; Lan, B.; Zhang, C.Z.; Cao, Y. Estrogen induces Vav1 expression in human breast cancer cells. *PLoS ONE* **2014**, *9*, e99052. [[CrossRef](#)]
99. Zhao, Z.; Zhang, K.-N.; Wang, Q.; Li, G.; Zeng, F.; Zhang, Y.; Wu, F.; Chai, R.; Wang, Z.; Zhang, C.; et al. Chinese Glioma Genome Atlas (CGGA): A Comprehensive Resource with Functional Genomic Data from Chinese Gliomas. *Genom. Proteom. Bioinform.* **2021**, *9*, 1–12. [[CrossRef](#)]
100. Gravendeel, L.A.M.; Kouwenhoven, M.C.M.; Gevaert, O.; de Rooij, J.J.; Stubbs, A.P.; Duijm, J.E.; Daemen, A.; Bleeker, F.E.; Bralten, L.B.C.; Kloosterhof, N.K.; et al. Intrinsic Gene Expression Profiles of Gliomas Are a Better Predictor of Survival than Histology. *Cancer Res.* **2009**, *69*, 9065. [[CrossRef](#)]
101. Cassetta, L.; Baekkevold, E.S.; Brandau, S.; Bujko, A.; Cassatella, M.A.; Dorhoi, A.; Krieg, C.; Lin, A.; Loré, K.; Marini, O.; et al. Deciphering myeloid-derived suppressor cells: Isolation and markers in humans, mice and non-human primates. *Cancer Immunol. Immunother. CII* **2019**, *68*, 687–697. [[CrossRef](#)]
102. Jave-Suarez, L.F.; Langbein, L.; Winter, H.; Praetzel, S.; Rogers, M.A.; Schweizer, J. Androgen regulation of the human hair follicle: The type I hair keratin hHa7 is a direct target gene in trichocytes. *J. Investig. Derm.* **2004**, *122*, 555–564. [[CrossRef](#)] [[PubMed](#)]
103. Burkart, M.F.; Wren, J.D.; Herschkowitz, J.I.; Perou, C.M.; Garner, H.R. Clustering microarray-derived gene lists through implicit literature relationships. *Bioinformatics* **2007**, *23*, 1995–2003. [[CrossRef](#)]
104. Chu, F.; Mason, K.E.; Anex, D.S.; Jones, A.D.; Hart, B.R. Hair Proteome Variation at Different Body Locations on Genetically Variant Peptide Detection for Protein-Based Human Identification. *Sci. Rep.* **2019**, *9*, 7641. [[CrossRef](#)] [[PubMed](#)]
105. Yoshida, H.; Taguchi, H.; Kitahara, T.; Takema, Y.; Visscher, M.O.; Schweizer, J.; Langbein, L. Keratins of the human occipital hair medulla: Androgenic regulation of in vitro hair keratin K37 expression. *Br. J. Derm.* **2013**, *169*, 218–221. [[CrossRef](#)] [[PubMed](#)]
106. Ke, X.; Chen, C.; Song, Y.; Cai, Q.; Li, J.; Tang, Y.; Han, X.; Qu, W.; Chen, A.; Wang, H.; et al. Hypoxia modifies the polarization of macrophages and their inflammatory microenvironment, and inhibits malignant behavior in cancer cells. *Oncol. Lett.* **2019**, *18*, 5871–5878. [[CrossRef](#)]
107. Canciello, A.; Russo, V.; Berardinelli, P.; Bernabò, N.; Muttini, A.; Mattioli, M.; Barboni, B. Progesterone prevents epithelial-mesenchymal transition of ovine amniotic epithelial cells and enhances their immunomodulatory properties. *Sci. Rep.* **2017**, *7*, 3761. [[CrossRef](#)] [[PubMed](#)]
108. Liu, Z.; Zhang, H.; Ding, S.; Qi, S.; Liu, S.; Sun, D.; Dong, W.; Yin, L.; Li, M.; Zhao, X.; et al.  $\beta$ Klotho inhibits androgen/androgen receptor-associated epithelial-mesenchymal transition in prostate cancer through inactivation of ERK1/2 signaling. *Oncol. Rep.* **2018**, *40*, 217–225. [[CrossRef](#)]
109. Velez-Perez, A.; Holder, M.K.; Fountain, S.; Blaustein, J.D. Estradiol Increases Microglial Response to Lipopolysaccharide in the Ventromedial Hypothalamus during the Peripubertal Sensitive Period in Female Mice. *Eneuro* **2020**, *7*, 0505-19. [[CrossRef](#)]
110. Contreras-Zárate, M.J.; Cittelly, D.M. Sex steroid hormone function in the brain niche: Implications for brain metastatic colonization and progression. *Cancer Rep.* **2020**, e1241. [[CrossRef](#)]
111. Aryanpour, R.; Pasbakhsh, P.; Zibara, K.; Namjoo, Z.; Beigi Boroujeni, F.; Shahbeigi, S.; Kashani, I.R.; Beyer, C.; Zendejdel, A. Progesterone therapy induces an M1 to M2 switch in microglia phenotype and suppresses NLRP3 inflammasome in a cuprizone-induced demyelination mouse model. *Int. Immunopharmacol.* **2017**, *51*, 131–139. [[CrossRef](#)]
112. Yao, P.-L.; Zhuo, S.; Mei, H.; Chen, X.-F.; Li, N.; Zhu, T.-F.; Chen, S.-T.; Wang, J.-M.; Hou, R.-X.; Le, Y.-Y. Androgen alleviates neurotoxicity of  $\beta$ -amyloid peptide (A $\beta$ ) by promoting microglial clearance of A $\beta$  and inhibiting microglial inflammatory response to A $\beta$ . *CNS Neurosci. Ther.* **2017**, *23*, 855–865. [[CrossRef](#)] [[PubMed](#)]
113. Su, E.J.; Ernst, L.; Abdallah, N.; Chatterton, R.; Xin, H.; Monsivais, D.; Coon, J.; Bulun, S.E. Estrogen receptor- $\beta$  and fetoplacental endothelial prostanoid biosynthesis: A link to clinically demonstrated fetal growth restriction. *J. Clin. Endocrinol. Metab.* **2011**, *96*, E1558–E1567. [[CrossRef](#)] [[PubMed](#)]
114. Tamura, M.; Deb, S.; Sebastian, S.; Okamura, K.; Bulun, S.E. Estrogen up-regulates cyclooxygenase-2 via estrogen receptor in human uterine microvascular endothelial cells. *Fertil. Steril.* **2004**, *81*, 1351–1356. [[CrossRef](#)] [[PubMed](#)]
115. Cianciaruso, C.; Beltraminelli, T.; Duval, F.; Nassiri, S.; Hamelin, R.; Mozes, A.; Gallart-Ayala, H.; Ceada Torres, G.; Torchia, B.; Ries, C.H.; et al. Molecular Profiling and Functional Analysis of Macrophage-Derived Tumor Extracellular Vesicles. *Cell Rep.* **2019**, *27*, 3062–3080.e11. [[CrossRef](#)]
116. Dou, C.; Ding, N.; Zhao, C.; Hou, T.; Kang, F.; Cao, Z.; Liu, C.; Bai, Y.; Dai, Q.; Ma, Q.; et al. Estrogen Deficiency-Mediated M2 Macrophage Osteoclastogenesis Contributes to M1/M2 Ratio Alteration in Ovariectomized Osteoporotic Mice. *J. Bone Miner. Res.* **2018**, *33*, 899–908. [[CrossRef](#)] [[PubMed](#)]
117. Tsai, Y.C.; Tseng, J.T.; Wang, C.Y.; Su, M.T.; Huang, J.Y.; Kuo, P.L. Medroxyprogesterone acetate drives M2 macrophage differentiation toward a phenotype of decidual macrophage. *Mol. Cell. Endocrinol.* **2017**, *452*, 74–83. [[CrossRef](#)] [[PubMed](#)]

118. Lang, Q.; Yidong, X.; Xueguang, Z.; Sixian, W.; Wenming, X.; Tao, Z. ETA-mediated anti-TNF- $\alpha$  therapy ameliorates the phenotype of PCOS model induced by letrozole. *PLoS ONE* **2019**, *14*, e0217495. [[CrossRef](#)]
119. Korbecki, J.; Olbromski, M.; Dziegiel, P. CCL18 in the Progression of Cancer. *Int. J. Mol. Sci.* **2020**, *21*, 7955. [[CrossRef](#)]
120. Tung, K.S.K.; Harakal, J.; Qiao, H.; Rival, C.; Li, J.C.H.; Paul, A.G.A.; Wheeler, K.; Pramoonjago, P.; Grafer, C.M.; Sun, W.; et al. Egress of sperm autoantigen from seminiferous tubules maintains systemic tolerance. *J. Clin. Investig.* **2017**, *127*, 1046–1060. [[CrossRef](#)]
121. Rival, C.; Wheeler, K.; Jeffrey, S.; Qiao, H.; Luu, B.; Tewalt, E.F.; Engelhard, V.H.; Tardif, S.; Hardy, D.; del Rio, R.; et al. Regulatory T cells and vasectomy. *J. Reprod. Immunol.* **2013**, *100*, 66–75. [[CrossRef](#)]
122. Wheeler, K.; Tardif, S.; Rival, C.; Luu, B.; Bui, E.; Del Rio, R.; Teuscher, C.; Sparwasser, T.; Hardy, D.; Tung, K.S. Regulatory T cells control tolerogenic versus autoimmune response to sperm in vasectomy. *Proc. Natl. Acad. Sci. USA* **2011**, *108*, 7511. [[CrossRef](#)]
123. Kessler, D.L.; Smith, W.D.; Hamilton, M.S.; Berger, R.E. Infertility in mice after unilateral vasectomy. *Fertil. Steril.* **1985**, *43*, 308–312. [[CrossRef](#)]
124. Tung, K.S.; Cooke, W.D., Jr.; McCarty, T.A.; Robitaille, P. Human sperm antigens and antisperm antibodies. II. Age-related incidence of antisperm antibodies. *Clin. Exp. Immunol.* **1976**, *25*, 73–79.
125. Mancini, R.E.; Andrada, J.A.; Saraceni, D.; Bachmann, A.E.; Lavieri, J.C.; Nemirovsky, M. Immunological and testicular response in man sensitized with human testicular homogenate. *J. Clin. Endocrinol. Metab.* **1965**, *25*, 859–875. [[CrossRef](#)]
126. Taguchi, O.; Nishizuka, Y. Experimental autoimmune orchitis after neonatal thymectomy in the mouse. *Clin. Exp. Immunol.* **1981**, *46*, 425–434.
127. Wong, A. The Molecular Evolution of Animal Reproductive Tract Proteins: What Have We Learned from Mating-System Comparisons? *Int. J. Evol. Biol.* **2011**, *2011*, 908735. [[CrossRef](#)]
128. Mahata, B.; Pramanik, J.; van der Weyden, L.; Polanski, K.; Kar, G.; Riedel, A.; Chen, X.; Fonseca, N.A.; Kundu, K.; Campos, L.S.; et al. Tumors induce de novo steroid biosynthesis in T cells to evade immunity. *Nat. Commun.* **2020**, *11*, 3588. [[CrossRef](#)] [[PubMed](#)]
129. The Cancer Genome Atlas Research Network. Comprehensive genomic characterization defines human glioblastoma genes and core pathways. *Nature* **2008**, *455*, 1061–1068. [[CrossRef](#)] [[PubMed](#)]
130. Yanguas-Casás, N. Physiological sex differences in microglia and their relevance in neurological disorders. *Neuroimmunol. Neuroinflamm.* **2020**, *7*, 13–22. [[CrossRef](#)]
131. Penning, T.M. Aldo-Keto Reductase (AKR) 1C3 inhibitors: A patent review. *Expert Opin. Pat.* **2017**, *27*, 1329–1340. [[CrossRef](#)]
132. Shibuya, R.; Suzuki, T.; Miki, Y.; Yoshida, K.; Moriya, T.; Ono, K.; Akahira, J.; Ishida, T.; Hirakawa, H.; Evans, D.B.; et al. Intratumoral concentration of sex steroids and expression of sex steroid-producing enzymes in ductal carcinoma in situ of human breast. *Endocr. Relat. Cancer* **2008**, *15*, 113–124. [[CrossRef](#)]
133. Zhou, J.; Wang, Y.; Wu, D.; Wang, S.; Chen, Z.; Xiang, S.; Chan, F.L. Orphan nuclear receptors as regulators of intratumoral androgen biosynthesis in castration-resistant prostate cancer. *Oncogene* **2021**, *40*, 2625–2634. [[CrossRef](#)] [[PubMed](#)]
134. Kamrath, C.; Hochberg, Z.; Hartmann, M.F.; Remer, T.; Wudy, S.A. Increased activation of the alternative “backdoor” pathway in patients with 21-hydroxylase deficiency: Evidence from urinary steroid hormone analysis. *J. Clin. Endocrinol. Metab.* **2012**, *97*, E367–E375. [[CrossRef](#)]
135. Chang, K.-H.; Li, R.; Papari-Zareei, M.; Watumull, L.; Zhao, Y.D.; Auchus, R.J.; Sharifi, N. Dihydrotestosterone synthesis bypasses testosterone to drive castration-resistant prostate cancer. *Proc. Natl. Acad. Sci. USA* **2011**, *108*, 13728–13733. [[CrossRef](#)]
136. Cai, C.; Balk, S.P. Intratumoral androgen biosynthesis in prostate cancer pathogenesis and response to therapy. *Endocr. Relat. Cancer* **2011**, *18*, R175–R182. [[CrossRef](#)] [[PubMed](#)]
137. Mohler, J.L.; Titus, M.A.; Wilson, E.M. Potential prostate cancer drug target: Bioactivation of androstenediol by conversion to dihydrotestosterone. *Clin. Cancer Res.* **2011**, *17*, 5844–5849. [[CrossRef](#)] [[PubMed](#)]
138. Oksala, R.; Karimaa, M.; Simola, O.; Ramela, M.; Riikonen, R.; Vehmaan-Kreula, P.; Rummakko, P.; Wohlfahrt, G.; Kallio, P.; Mustonen, M.V.J. CYP11A1 inhibition as a therapeutic approach for the treatment of castration resistant prostate cancer. *J. Clin. Oncol.* **2018**, *36*, 340. [[CrossRef](#)]
139. Dutt, S.S.; Gao, A.C. Molecular mechanisms of castration-resistant prostate cancer progression. *Future Oncol.* **2009**, *5*, 1403–1413. [[CrossRef](#)]
140. O'Donnell, A.; Judson, I.; Dowsett, M.; Raynaud, F.; Dearnaley, D.; Mason, M.; Harland, S.; Robbins, A.; Halbert, G.; Nutley, B.; et al. Hormonal impact of the 17 $\alpha$ -hydroxylase/C(17,20)-lyase inhibitor abiraterone acetate (CB7630) in patients with prostate cancer. *Br. J. Cancer* **2004**, *90*, 2317–2325. [[CrossRef](#)] [[PubMed](#)]
141. Girish, V.; Vijayalakshmi, A. Affordable image analysis using NIH Image/ImageJ. *Indian J. Cancer* **2004**, *41*, 47.
142. Sharpe, M.A.; Baskin, D.S. Monoamine oxidase B levels are highly expressed in human gliomas and are correlated with the expression of HiF-1 $\alpha$  and with transcription factors Sp1 and Sp3. *Oncotarget* **2016**, *7*, 3379–3393. [[CrossRef](#)] [[PubMed](#)]
143. Carmona, L.M.; Schatz, D.G. New insights into the evolutionary origins of the recombination-activating gene proteins and V(D)J recombination. *FEBS J.* **2017**, *284*, 1590–1605. [[CrossRef](#)] [[PubMed](#)]
144. Gutcher, I.; Becher, B. APC-derived cytokines and T cell polarization in autoimmune inflammation. *J. Clin. Investig.* **2007**, *117*, 1119–1127. [[CrossRef](#)] [[PubMed](#)]
145. Zarnitsyna, V.I.; Evavold, B.D.; Schoettle, L.N.; Blattman, J.N.; Antia, R. Estimating the diversity, completeness, and cross-reactivity of the T cell repertoire. *Front. Immunol.* **2013**, *4*, 485. [[CrossRef](#)]

146. Mora, T.; Walczak, A.M. How many different clonotypes do immune repertoires contain? *Curr. Opin. Syst. Biol.* **2019**, *18*, 104–110. [[CrossRef](#)]
147. Wang, W.; Thomas, R.; Sizova, O.; Su, D.M. Thymic Function Associated With Cancer Development, Relapse, and Antitumor Immunity—A Mini-Review. *Front. Immunol.* **2020**, *11*, 773. [[CrossRef](#)]
148. Gotot, J.; Gottschalk, C.; Leopold, S.; Knolle, P.A.; Yagita, H.; Kurts, C.; Ludwig-Portugall, I. Regulatory T cells use programmed death 1 ligands to directly suppress autoreactive B cells in vivo. *Proc. Natl. Acad. Sci. USA* **2012**, *109*, 10468–10473. [[CrossRef](#)]
149. Dal Secco, V.; Riccioli, A.; Padula, F.; Ziparo, E.; Filippini, A. Mouse Sertoli cells display phenotypical and functional traits of antigen-presenting cells in response to interferon gamma. *Biol. Reprod.* **2008**, *78*, 234–242. [[CrossRef](#)]
150. Kisand, K.; Peterson, P. Autoimmune polyendocrinopathy candidiasis ectodermal dystrophy: Known and novel aspects of the syndrome. *Ann. N. Y. Acad. Sci.* **2011**, *1246*, 77–91. [[CrossRef](#)]
151. O'Donnell, L.; Rebourcet, D.; Dagley, L.F.; Sgaier, R.; Infusini, G.; O'Shaughnessy, P.J.; Chalmel, F.; Fietz, D.; Weidner, W.; Legrand, J.M.D.; et al. Sperm proteins and cancer-testis antigens are released by the seminiferous tubules in mice and men. *FASEB J.* **2021**, *35*, e21397. [[PubMed](#)]
152. Fijak, M.; Pilatz, A.; Hedger, M.P.; Nicolas, N.; Bhushan, S.; Michel, V.; Tung, K.S.K.; Schuppe, H.-C.; Meinhardt, A. Infectious, inflammatory and 'autoimmune' male factor infertility: How do rodent models inform clinical practice? *Hum. Reprod. Update* **2018**, *24*, 416–441. [[CrossRef](#)] [[PubMed](#)]
153. Feng, Z.Y.; Ming, W.; Li, L.D.; Louis, J.; Fei, W.Y. Adoptive transfer of murine autoimmune orchitis with sperm-specific T lymphoblasts. *Arch. Androl.* **1990**, *24*, 51–59. [[CrossRef](#)]
154. Al-Fahham, A.A. Etiology of Antisperm Antibodies in the Serum of Virgins. *Open J. Obstet. Gynecol.* **2018**, *8*, 236–245. [[CrossRef](#)]
155. Mahdi, B.M.; Salih, W.H.; Caitano, A.E.; Kadhum, B.M.; Ibrahim, D.S. Frequency of antisperm antibodies in infertile women. *J. Reprod. Infertil.* **2011**, *12*, 261–265.
156. Robertson, S.A.; Prins, J.R.; Sharkey, D.J.; Moldenhauer, L.M. Seminal Fluid and the Generation of Regulatory T Cells for Embryo Implantation. *Am. J. Reprod. Immunol.* **2013**, *69*, 315–330. [[CrossRef](#)]
157. Robertson, S.A.; Guerin, L.R.; Moldenhauer, L.M.; Hayball, J.D. Activating T regulatory cells for tolerance in early pregnancy—The contribution of seminal fluid. *J. Reprod. Immunol.* **2009**, *83*, 109–116. [[CrossRef](#)]
158. Remes Lenicov, F.; Rodriguez Rodrigues, C.; Sabatté, J.; Cabrini, M.; Jancic, C.; Ostrowski, M.; Merlotti, A.; Gonzalez, H.; Alonso, A.; Pasqualini, R.A.; et al. Semen Promotes the Differentiation of Tolerogenic Dendritic Cells. *J. Immunol.* **2012**, *189*, 4777–4786. [[CrossRef](#)]
159. Remes Lenicov, F.; Paletta, A.L.; Gonzalez Prinz, M.; Varese, A.; Pavillet, C.E.; Lopez Malizia, Á.; Sabatté, J.; Geffner, J.R.; Ceballos, A. Prostaglandin E2 Antagonizes TGF- $\beta$  Actions During the Differentiation of Monocytes Into Dendritic Cells. *Front. Immunol.* **2018**, *9*, 1441. [[CrossRef](#)] [[PubMed](#)]
160. Bruno, A.; Mortara, L.; Baci, D.; Noonan, D.M.; Albini, A. Myeloid Derived Suppressor Cells Interactions With Natural Killer Cells and Pro-angiogenic Activities: Roles in Tumor Progression. *Front. Immunol.* **2019**, *10*, 771. [[CrossRef](#)]
161. Obermajer, N.; Kalinski, P. Generation of myeloid-derived suppressor cells using prostaglandin E2. *Transplant. Res.* **2012**, *1*, 15. [[CrossRef](#)] [[PubMed](#)]
162. Bendvold, E.; Gottlieb, C.; Svanborg, K.; Bygdeman, M.; Eneroth, P. Concentration of prostaglandins in seminal fluid of fertile men. *Int. J. Androl.* **1987**, *10*, 463–469. [[CrossRef](#)] [[PubMed](#)]
163. Sumida, K.; Ohno, Y.; Ohtake, J.; Kaneumi, S.; Kishikawa, T.; Takahashi, N.; Taketomi, A.; Kitamura, H. IL-11 induces differentiation of myeloid-derived suppressor cells through activation of STAT3 signalling pathway. *Sci. Rep.* **2015**, *5*, 13650. [[CrossRef](#)] [[PubMed](#)]
164. Liu, M.; Li, S.; Li, M.O. TGF- $\beta$  Control of Adaptive Immune Tolerance: A Break from Treg Cells. *BioEssays News Rev. Mol. Cell Dev. Biol.* **2018**, *40*, e1800063. [[CrossRef](#)]
165. Chen, J.C.; Johnson, B.A.; Erikson, D.W.; Piltonen, T.T.; Barragan, F.; Chu, S.; Kohgadari, N.; Irwin, J.C.; Greene, W.C.; Giudice, L.C.; et al. Seminal plasma induces global transcriptomic changes associated with cell migration, proliferation and viability in endometrial epithelial cells and stromal fibroblasts. *Hum. Reprod.* **2014**, *29*, 1255–1270. [[CrossRef](#)]
166. Qureshi, O.S.; Zheng, Y.; Nakamura, K.; Attridge, K.; Manzotti, C.; Schmidt, E.M.; Baker, J.; Jeffery, L.E.; Kaur, S.; Briggs, Z.; et al. Trans-endocytosis of CD80 and CD86: A molecular basis for the cell-extrinsic function of CTLA-4. *Science* **2011**, *332*, 600–603. [[CrossRef](#)]
167. Kowalczyk, A.; D'Souza, C.A.; Zhang, L. Cell-extrinsic CTLA4-mediated regulation of dendritic cell maturation depends on STAT3. *Eur. J. Immunol.* **2013**, *44*, 1143–1155. [[CrossRef](#)] [[PubMed](#)]
168. Jørgensen, N.; Persson, G.; Hviid, T.V.F. The Tolerogenic Function of Regulatory T Cells in Pregnancy and Cancer. *Front. Immunol.* **2019**, *10*, 911. [[CrossRef](#)] [[PubMed](#)]
169. Tsuda, S.; Nakashima, A.; Shima, T.; Saito, S. New Paradigm in the Role of Regulatory T Cells during Pregnancy. *Front. Immunol.* **2019**, *10*, 573. [[CrossRef](#)]
170. Baskin, M.J. Temporary sterilization by the injection of human spermatozoa. A preliminary report. *Am. J. Obstet. Gynecol.* **1932**, *24*, 892–897. [[CrossRef](#)]
171. Kaur, K.; Prabha, V. Immunocontraceptives: New approaches to fertility control. *BioMed Res. Int.* **2014**, *2014*, 868196. [[CrossRef](#)] [[PubMed](#)]